EurJIC
European Journal of Inorganic Chemistry

Full Papers
doi.org/10.1002/ejic.202100629

Chemistry Europe
European Chemical Societies Publishing

VIP *Very Important Paper*

Special Issue

Reactivity of Terminal Iron Borylenes and Bis(borylenes) with Carbodiimides: Cycloaddition, Metathesis, Insertion and C–H Activation Pathways

Alexander Matler,[a, b] Merle Arrowsmith,[a, b] Fabian Schorr,[a, b] Alexander Hermann,[a, b] Alexander Hofmann,[a, b] Carsten Lenczyk,[a, b] and Holger Braunschweig*[a, b]

The reactions of carbodiimides with the iron arylborylene complex [Fe=BDur(CO)$_3$(PMe$_3$)] (Dur = 2,3,5,6-Me$_4$C$_6$H) and the iron bis(borylene) complex [Fe{=BDur}{=BN(SiMe$_3$)$_2$}(CO)$_3$] yield a wide variety of temperature-dependent products, including known FeBNC and novel FeBNB metallacycles, complexes of N-heterocyclic boracarbene and spiro-boracarbene ligands and a unique 1,3,2,4-diazadiborolyl pianostool complex, characterized by NMR spectroscopy and X-ray crystallography. The product distributions can be rationalized by considering sequences of cycloaddition, metathesis, insertion, and C–H activation pathways mainly governed by sterics.

Introduction

Since the isolation of the first terminal transition metal borylene complexes of the form [L$_n$M=BR] in 1998,[1] their chemistry has been extensively explored, revealing reactivity patterns similar to those found in metal alkylidene chemistry, including insertion, metathesis and borylene transfer reactions.[2] Unlike metal alkylidene metathesis reactions, borylene metathesis reactions require a substrate with a polarized multiple bond to proceed. In 2005 Aldridge and co-workers reported the first metathesis reaction involving the M=B and E=Y bonds of the cationic iron aminoborylene [CpFe=BN*i*Pr$_2$(CO)$_2$]$^+$ (Cp = η^5-C$_5$H$_5$) and Ph$_3$E=Y (E = P, Y = O, S; E = As, Y = O), respectively, yielding [CpFeEPh$_3$(CO)$_2$]$^+$ and the corresponding boroxine or 1,3-dithia-2,4-diboretanes, derived from the oligomerization of the kinetically unstable [YBN*i*Pr$_2$] metathesis products (Scheme 1a).[3] The reaction with Ph$_3$PO was shown to proceed via a two-step mechanism, the first being the coordination of the phosphine oxide as a Lewis base at the electron-deficient boron center of the iron borylene.[3] We later showed that the reaction with Ph$_3$PS proceeds differently, via the formation of a metallathiaborirane and liberation of Ph$_3$P.[4] The first concerted metathesis reaction of a terminal metal borylene was reported by our group between the manganese alkylborylene [CpMn=B*t*Bu(CO)$_2$] and benzophenone, resulting in the formation of the Fisher-type carbene complex [CpMn=CPh$_2$(CO)$_2$] and the boroxine (OB*t*Bu)$_3$, which is the trimer of the unstable oxoborane metathesis product [OB*t*Bu] (Scheme 1b).[5] The intermediate [2 + 2] cycloaddition complex was isolated from the reactions of several benzophenone derivatives with [CpMn=B*t*Bu(CO)$_2$][4,5] and [Fe=BDur(CO)$_3$(PMe$_3$)] (Dur = 2,3,5,6-Me$_4$C$_6$H), complex **I** (Scheme 2),[6] respectively.

A similar reaction pattern was also observed between [CpFe=BN*i*Pr$_2$(CO)$_2$]$^+$ and phenylisocyanate: after a [2 + 2] cycloaddition step, a cycloreversion step yielded the cationic metal isonitrile complex and the boroxine (OBN*i*Pr$_2$)$_3$ as the metathesis products (Scheme 1c).[7] More complex reactivity patterns have been observed between manganese or iron borylenes and carbodiimides. After an initial cycloaddition step that yields a MBNC metallacycle with a pendant imine functionality, which can be isolated in the case of the reaction between [Cp(CO)$_2$Mn=B*t*Bu] and dicyclohexylcarbodiimide (DCC),[5] a rearrangement leads to the formation of a metal-bound carbene-like 1,3-diaza-4-boretidin-2-yl ligand (Scheme 1d).[4,8] In the case of the cationic iron iminoborylene complex [CpFe=B=N=CMes$_2$(CO)(PCy$_3$)]$^+$ (Mes = 2,4,6-Me$_3$C$_6$H$_2$) and the neutral chromium arylborylenes [Cr=BAr(CO)$_5$] (Ar = 2,6-(2,4,6-R$_3$C$_6$H$_2$)C$_6$H$_3$, R = Me, *i*Pr) this rearrangement was followed by the formation of the reactive cumulene [RN=B=N=CMes$_2$][7a] and iminoborane [RN≡BAr][9] metathesis products (R = *i*Pr, Cy), respectively, which both undergo a subsequent cycloaddition reaction with a second equivalent of carbodiimide (Scheme 1e). For the cationic iron aminoborylene [CpFe=BN*i*Pr$_2$(CO)$_2$]$^+$ the intermediate 1,3-diaza-4-boretidin-2-yl complex undergoes a second insertion reaction of a carbodiimide into the B–N*i*Pr$_2$ bond, leading to the formation of a stable iron complex with a spirocyclic boracarbene ligand (Scheme 1f).[8] Attempts to achieve metal borylene metathesis with other polar unsaturated

[a] Dr. A. Matler, Dr. M. Arrowsmith, F. Schorr, Dr. A. Hermann, Dr. A. Hofmann, Dr. C. Lenczyk, Prof. Dr. H. Braunschweig
Institute for Inorganic Chemistry,
Julius-Maximilians-Universität Würzburg,
Am Hubland, 97074 Würzburg, Germany
E-mail: h.braunschweig@uni-wuerzburg.de
[b] Dr. A. Matler, Dr. M. Arrowsmith, F. Schorr, Dr. A. Hermann, Dr. A. Hofmann, Dr. C. Lenczyk, Prof. Dr. H. Braunschweig
Institute for Sustainable Chemistry & Catalysis with Boron,
Julius-Maximilians-Universität Würzburg,
Am Hubland, 97074 Würzburg, Germany

Supporting information for this article is available on the WWW under https://doi.org/10.1002/ejic.202100629

Special Issue Board Member Virtual Issue

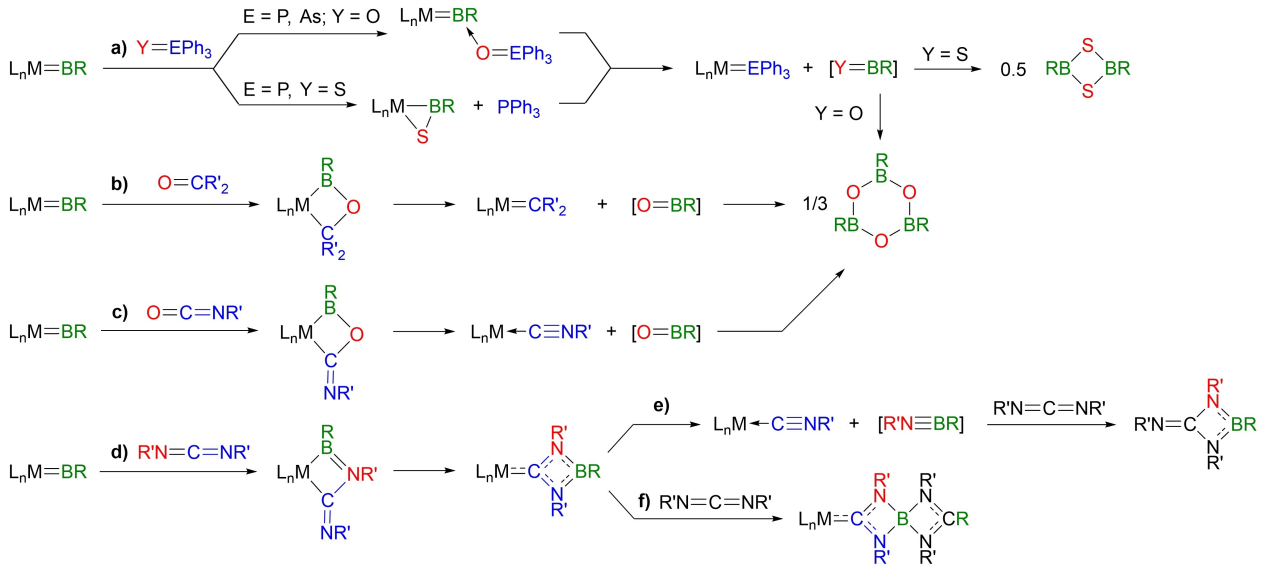

Scheme 1. Metathesis and insertion reactions of transition metal borylenes with polarized double bonds.

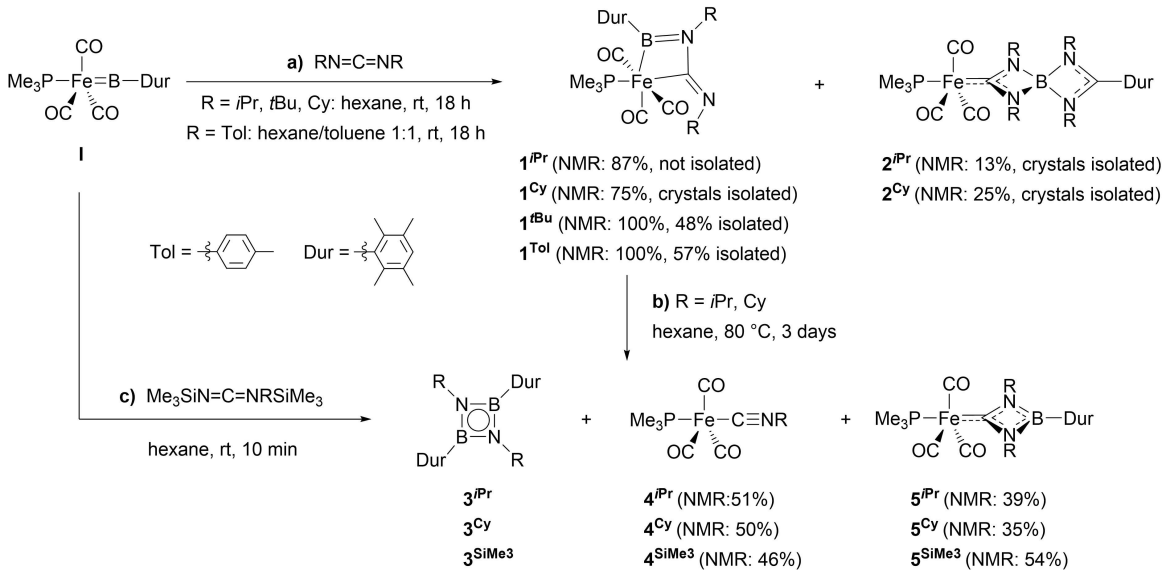

Scheme 2. Reactions of the iron arylborylene complex **I** with carbodiimides.

substrates, such as iminophosphines or isonitriles, only led to the insertion of the latter into the metal-boron bond.[10]

In comparison, the reactivity of bis(borylene) metal complexes towards unsaturated substrates has been relatively underexplored. Upon addition of one or two phosphine ligands the iron bis(borylene) complex [Fe{=BDur}{=BN(SiMe$_3$)$_2$}(CO)$_3$] (**II**, Scheme 4)[11] undergoes insertion of one or two CO ligands into one or both of the Fe–B bonds, respectively.[12] Furthermore, complex **II** can transfer both borylene fragments to internal alkynes to yield 1,4-diborabutadiene and 1,4-diborahexadiene complexes,[13] the former undergoing cyclization with both atoms of CO upon addition of CO and PMe$_3$.[14] The reactivity of **II** towards heterocumulenes, however, has yet to be explored, and there have been no reports of metathesis reactions with **II**.

In this work we study the versatile reactivity of the neutral iron arylborylene complex **I** and of the iron bis(borylene) complex **II** towards a range of carbodiimides, which include cycloaddition, metathesis and insertion reactions, as well as the unprecedented formation of a 1,3,2,4-diazadiborolyl ligand with two different coordination modes.

Results and Discussion

Reactions of an iron durylborylene complex with carbodiimides

*Reactions with di-*tert*-butyl- and di-*p*-tolylcarbodiimide*

The reactions of the phosphine-stabilized terminal iron durylborylene complex **I** with one equivalent of di-*tert*-butyl- and di-*p*-tolylcarbodiimide proceeded selectively at room temperature overnight to yield the colorless complexes $\mathbf{1}^{tBu}$ and $\mathbf{1}^{Tol}$, respectively, which result from the [2 + 2] cycloaddition of the carbodiimide C=N double bond with the Fe=B double bond (Scheme 2a). The broad ^{11}B NMR resonances of $\mathbf{1}^{tBu}$ and $\mathbf{1}^{Tol}$ appear at 65.7 and 69.3 ppm, respectively, and their ^{31}P NMR resonances at 9.1 and 11.5 ppm, respectively. These shifts are similar to those of the related cycloaddition product between **I** and 2-adamantanone (δ_{11B} = 72.6 ppm; δ_{31P} = 11.1 ppm),[4] which presents a very similar coordination sphere, with an FeBOC ring instead of an FeBNC ring. The ^{13}C{^{1}H} NMR spectra show two characteristically deshielded, broad *C*O resonances in the 212–216 ppm region, corresponding to the CO ligands *trans* and *cis* to the boryl fragment. For $\mathbf{1}^{tBu}$ a doublet at 151.6 ppm ($^2J_{CP}$ = 10.5 Hz) was attributed to the iron-bound central carbon atom of the carbodiimide moiety, coupling to the phosphorus atom in *trans*. The corresponding ^{13}C{^{1}H} NMR resonance for $\mathbf{1}^{Tol}$ at 169.0 ppm was so broadened by coupling to the quadrupolar boron nucleus that it was only detectable by HMBC. It is significantly downfield-shifted from that of $\mathbf{1}^{tBu}$, reflecting the electron-withdrawing nature of the *p*-tolyl substituent. The solid-state IR spectra of $\mathbf{1}^{tBu}$ and $\mathbf{1}^{Tol}$ show two sets of CO stretching bands in the 2020–2030 cm^{-1} and 1935–1980 cm^{-1} regions, similar to the iron silyl boryl complex [Fe(BClDur)(SiMe$_3$)(CO)$_3$(PMe$_3$)] (υ_{CO} = 2025, 1946).[15] The cycloaddition of DCC to transition metal borylenes has been observed with the manganese alkylborylene [CpMn=B*t*Bu(CO)$_2$][4,5] at room temperature, and with the cationic iron iminoborylene [CpFe=B=N=CMes$_2$(CO)(PCy$_3$)]$^+$ at low temperatures (Scheme 1d).[7] Complexes $\mathbf{1}^{tBu}$ and $\mathbf{1}^{Tol}$ were further characterized by X-ray crystallographic analyses (see Figures S38 and S39 in the Supporting Information).

*Reactions with di*isopropyl*- and dicyclohexylcarbodiimide*

In contrast, the reactions of **I** with one equivalent of di*iso*propylcarbodiimide (DIC) or DCC at rt overnight yielded a mixture of two products (Scheme 2a). ^{11}B and ^{31}P NMR-spectroscopic analyses showed the formation of the cycloaddition products $\mathbf{1}^{iPr}$ (87%, δ_{11B} = 63.2 ppm; δ_{31P} = 10.2 ppm) and $\mathbf{1}^{Cy}$ (75%, δ_{11B} = 63.3 ppm; δ_{31P} = 10.4 ppm), alongside the complexes $\mathbf{2}^{iPr}$ (13%, δ_{11B} = 6.6 ppm; δ_{31P} = 39.3 ppm) and $\mathbf{2}^{Cy}$ (25%, δ_{11B} = 6.9 ppm; δ_{31P} = 39.6 ppm), respectively, resulting from the insertion of a carbodiimide unit into both the Fe–B and the B–C$_{Dur}$ bonds of **I**. While $\mathbf{1}^{Cy}$ could be isolated as an analytically pure colorless solid by fractional crystallization at −30 °C, the products of the reaction with DIC could not be separated satisfactorily. Aldridge and co-workers have reported a similar insertion of DCC into both the Fe=B and B=N bonds of the cationic iron aminoborylene [CpFe=B=NCy$_2$(CO)$_2$]$^+$, yielding a spiro complex analogous to $\mathbf{2}^{iPr}$ and $\mathbf{2}^{Cy}$ (Scheme 1f).[8] Complexes $\mathbf{2}^{iPr}$, $\mathbf{1}^{Cy}$ and $\mathbf{2}^{Cy}$ were further characterized by X-ray crystallographic analyses (Figure 2 and Figure S41 in the Supporting Information).

Heating these product mixtures for 3 days at 80 °C resulted in ca. 90% conversion to a new product mixture (Scheme 2b). ^{11}B NMR spectra showed the broad resonances of the iminoborane dimers (DurBNR)$_2$, $\mathbf{3}^{iPr}$ (δ_{11B} = 44.0 ppm) and $\mathbf{3}^{Cy}$ (δ_{11B} = 44.6 ppm), assigned by comparison to (PhBN*t*Bu)$_2$ (δ_{11B} = 42.5 ppm),[16] which result from the cycloreversion of $\mathbf{1}^{R}$, i.e. the formal metathesis between **I** and the carbodiimides. The second product of these cycloreversion reactions, the isonitrile complexes [Fe(C≡NR)(CO)$_3$(PMe$_3$)] ($\mathbf{4}^{R}$) were detected in the ^{31}P NMR spectra at ca. 38.5 ppm. Similarly, our group has reported that a chromium terphenylborylene derivative undergoes metathesis with DIC and DCC to yield transient iminoborane monomers, detectable by ^{11}B NMR spectroscopy, which, instead of dimerizing as in our case, undergo a cycloaddition reaction with excess DCC (Scheme 1e).[7b] A third thermolysis product was identified as $\mathbf{5}^{R}$ (δ_{11B} ca. 42 ppm; δ_{31P} ca. 38.0 ppm), which results from the rearrangement of $\mathbf{1}^{R}$. The analogous thermal rearrangement of a 1-metalla-3,4-azaboretidine-4-imine to a 1,3,4-diazaboretidin-2-yl metal complex had been observed for the cycloaddition product of DCC with [CpMn=B*t*Bu(CO)$_2$] (δ_{11B} = 47 ppm)[3] and the cationic iron complex [CpFe=B=NCy$_2$(CO)(PCy$_3$)]$^+$ (δ_{11B} = 25 ppm).[8a,b] Our group and that of Aldridge have shown that the 1,3,4-diazaboretidin-2-yl ligands of $\mathbf{2}^{R}$ and $\mathbf{5}^{R}$ have carbenoid character,[3,8a,c] making them related to N-heterocyclic carbenes (NHCs, Figure 1). Their ^{31}P NMR shift in the 38–40 ppm range is upfield of that of the related phosphine-NHC complex *trans*-[Fe(CO)$_3$(IMes)(PMe$_3$)] (IMes = 1,3-bis(2,4,6-trimethylphenyl) imidazol-2-ylidene, δ_{31P} = 45.9 ppm)[17] and similar to that of *trans*-[Fe(CO)$_3$(PMe$_3$)$_2$] (δ_{31P} = 38.5 ppm),[18] suggesting a donor strength higher than that of NHCs and similar to that of PMe$_3$.

Reaction with bis(trimethylsilyl)carbodiimide

Finally, bis(trimethylsilyl)carbodiimide reacted with **I** within less than 10 min at room temperature (Scheme 2c) to yield a mixture of the iminoborane dimer (DurBNSiMe$_3$)$_2$, $\mathbf{3}^{SiMe3}$ (δ_{11B} = 47 ppm, similar to (MesB=NSiMe$_3$)$_2$: δ_{11B} = 45.0 ppm),[19] and a 46:54 mixture of the iron complexes $\mathbf{4}^{SiMe3}$ and $\mathbf{5}^{SiMe3}$. Like their *iso*propyl and cyclohexyl analogues these are presumably formed via a transient cycloaddition complex $\mathbf{1}^{SiMe3}$. The formation of $\mathbf{3}^{SiMe3}$ was further confirmed by a single-crystal X-

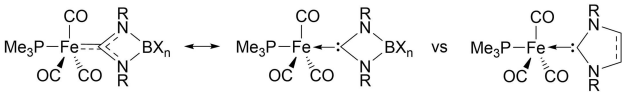

Figure 1. Analogy between 1,3,4-diazaboretidin-2-yl and NHC ligands.

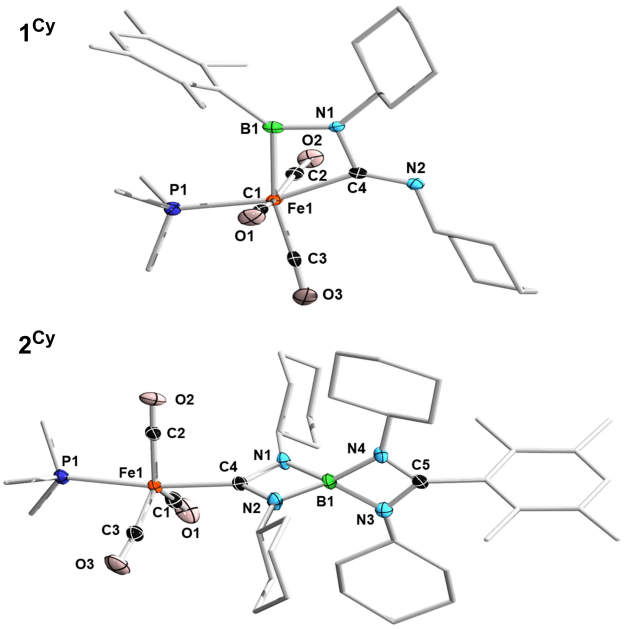

Figure 2. Crystallographically-derived solid-state structures of $\mathbf{1}^{Cy}$ and $\mathbf{2}^{Cy}$. Atomic displacement ellipsoids drawn at 50% probability level. Ellipsoids on the ligand periphery and hydrogen atoms omitted for clarity.

ray crystallographic analysis (see Figure S50 in the Supporting Information).

Postulated reaction mechanisms

Based on previous experimental and theoretical results from our group and that of Aldridge,[3–8] it is possible to postulate the mechanism of the reactions of **I** with carbodiimides (Scheme 3). The insertion of the first equivalent of carbodiimide into the Fe=B bond proceeds via the cycloaddition intermediate $\mathbf{1}^{R}$, followed by thermally-induced Fe–B bond cleavage to yield **Int1** (step i) and ring closure between the dicoordinate boron center and the pendant imino nitrogen atom to yield $\mathbf{5}^{R}$ (step ii).[8b] The formation of $\mathbf{5}^{R}$ from $\mathbf{1}^{R}$ had been confirmed experimentally by the thermal rearrangement of the cycloaddition product between [CpMn=B*t*Bu(CO)$_2$] and DCC, which yielded the product of the formal insertion of DCC into the original Mn=B bond.[4] The second insertion of carbodiimide then proceeds by adduct formation at the boron center to yield **Int2** (step iii), followed by insertion of a C=N bond into the B–R′ bond to yield **Int3** (step iv), and finally another ring closure between the tricoordinate boron center and the pendant imino-nitrogen to yield $\mathbf{2}^{R}$ (step v).[8b] The reason why the reactions of **I** with DCC and DIC lead to the mixtures of $\mathbf{1}^{R}$ and $\mathbf{2}^{R}$, whereas those with di-*tert*-butylcarbodiimide and di-*p*-tolylcarbodiimide selectively yield $\mathbf{1}^{R}$ only, may be due to steric repulsion between the *t*Bu and Dur fragments preventing the rearrangement to $\mathbf{5}^{R}$ in the case of the *tert*-butyl derivative, and electronic stabilization of $\mathbf{1}^{R}$ by the electron-withdrawing tolyl group in the case of the *p*-tolyl derivative. Alternatively, $\mathbf{1}^{R}$ can undergo a cycloreversion reaction (step vi), forming the borylene metathesis products, the iron isonitrile complex $\mathbf{4}^{R}$ and the monomeric iminoborane **Int4**,[7] which dimerizes to $\mathbf{3}^{R}$ (step vii). In the case of the trimethylsilyl derivative the combined steric demands and electron-donating nature of the SiMe$_3$ group destabilize $\mathbf{1}^{SiMe3}$, while the iminoborane **Int4** is kinetically stabilized, thus favoring a spontaneous cycloreversion process.

Reactions of an iron bis(borylene) complex with carbodiimides

Reactions with DIC and DCC

The reaction of DIC and DCC with the iron bis(borylene) complex **II** proceeded cleanly at room temperature to yield the colorless diboryl complexes $\mathbf{6}^{iPr}$ and $\mathbf{6}^{Cy}$, respectively (Scheme 4a). The ^{11}B NMR spectra of $\mathbf{6}^{iPr}$ and $\mathbf{6}^{Cy}$ show two broad resonances at ca. 68 and 51 ppm, for the *B*Dur and *B*N(SiMe$_3$)$_2$ moieties, respectively. For $\mathbf{6}^{iPr}$ the ^{13}C{^{1}H} NMR resonance of the CO ligands *cis* to the diboryl ligand appear at 215.6 ppm, while the resonances of the *C*O *trans* to the BDur moiety and of *C*≡N*i*Pr *trans* to the *B*N(SiMe$_3$)$_2$ moiety are too broadened by coupling to the quadrupolar boron nuclei to detect. The solid-state IR spectra of $\mathbf{6}^{iPr}$ and $\mathbf{6}^{Cy}$ show a set of characteristic C≡N stretching bands in the 2130–2165 cm^{-1} region. The C≡O stretching bands are divided into two sets, with one band around 2000 cm^{-1} and the others in the 1885–1940 cm^{-1}

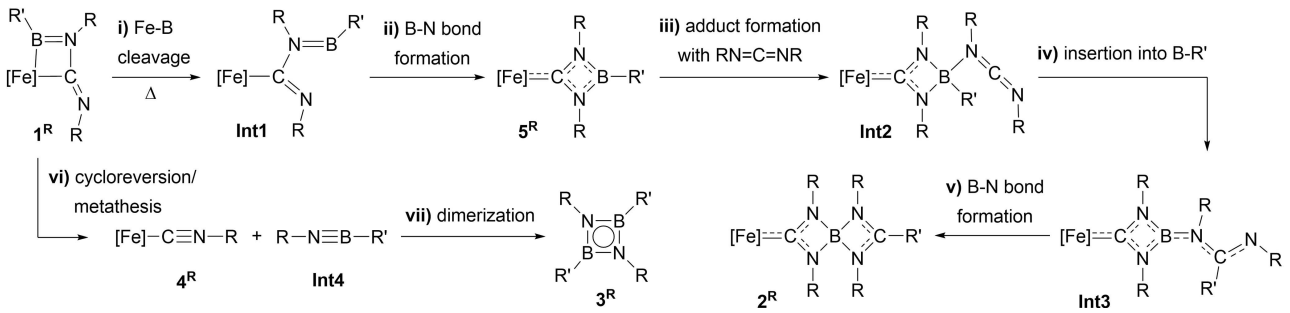

Scheme 3. Postulated mechanism of formation of compounds $\mathbf{2}^{R}$–$\mathbf{5}^{R}$. [Fe]=Fe(CO)$_3$(PMe$_3$).

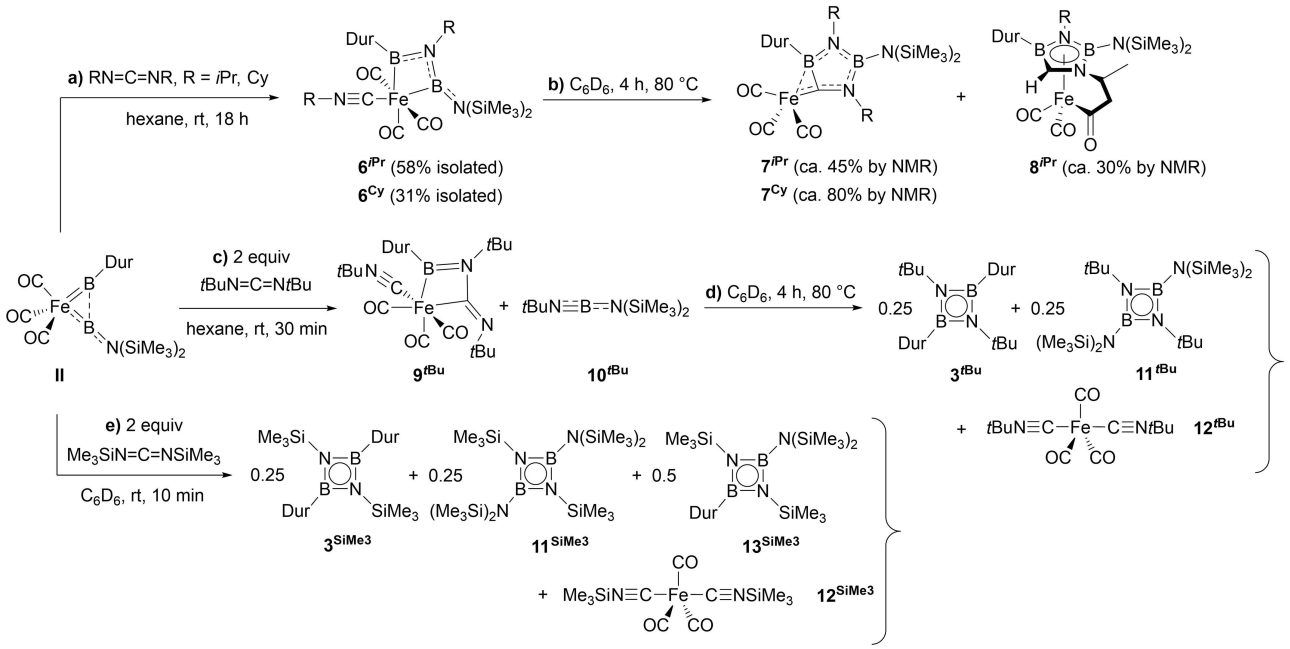

Scheme 4. Reactions of the iron bis(borylene) complex **II** with carbodiimides.

region, all shifted to lower wavelengths than in $\mathbf{1}^{tBu}$ and $\mathbf{1}^{Tol}$ (υ_{CO} = 2020–2030, 1935–1980 cm^{-1}). Complexes $\mathbf{6}^{iPr}$ and $\mathbf{6}^{Cy}$ were characterized by X-ray crystallographic analyses (Figure 3 and Figure S44 in the Supporting Information) and are the first metal complexes of a chelating, dianionic diborylamine ligand of the form $[R'BN(R)BR'']^{2-}$.

Thermolysis of 6^R

Heating $\mathbf{6}^{iPr}$ and $\mathbf{6}^{Cy}$ in C_6D_6 at 80 °C for several hours resulted in complete conversion to new product mixtures (Scheme 4b). In the case of $\mathbf{6}^{Cy}$ the major product, $\mathbf{7}^{Cy}$ (ca. 80% by NMR), presents two broad ^{11}B NMR resonances at 41.8 (*B*Dur) and 33.6 (*B*N($SiMe_3$)$_2$) ppm. An X-ray crystallographic analysis of dark-red single crystals of $\mathbf{7}^{Cy}$ obtained by fractional crystallization identified it as the product of the insertion of the isonitrile C≡N bond into both Fe–B bonds, which generates an iron-bound 1,3,2,4-diazadiborol-5-ylidene heterocycle (see Figure S46 in the Supporting Information). Unfortunately, the formation of several unidentified byproducts (ca. 20%) and the instability of $\mathbf{7}^{Cy}$ in solution prevented its clean isolation for further analyses.

In the case of $\mathbf{6}^{iPr}$, the ^1H and ^{11}B NMR spectra showed, beside the formation of $\mathbf{7}^{iPr}$ as the major product (ca. 45%, δ_{11B} = 41.1 (*B*Dur), 33.1 (*B*N($SiMe_3$)$_2$) ppm, see Figure 3 for the solid-state structure of $\mathbf{7}^{iPr}$), another product formed in ca. 30% yield, complex $\mathbf{8}^{iPr}$ (Scheme 4b). The ^{11}B NMR resonances of $\mathbf{8}^{iPr}$ are shifted significantly upfield from $\mathbf{7}^{iPr}$ to 29.6 (*B*Dur) and 21.0 (*B*N($SiMe_3$)$_2$) ppm. An X-ray crystallographic analysis of orange single crystals of $\mathbf{8}^{iPr}$ obtained by fractional crystallization identified it as an iron(II) piano-stool complex with a unique η^5-1,3,2,4-diazadiborolyl ligand chelating the iron center by a pendant 3-*N*-butanoyl side arm (Figure 3). Complex $\mathbf{8}^{iPr}$ is the first example of a complex with an η^5-1,3,2,4-diazadiborolyl ligand. The only known diazadiborolyl complexes are those of the 1,2,3,5-isomer, of which an iron sandwich complex has also been synthesized by the group of Roesler, who showed that these ligands are more electron-rich than cyclopentadienyls.[20]

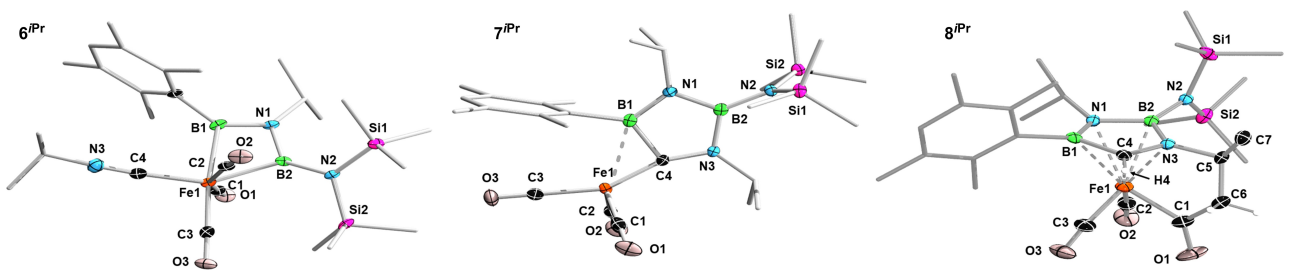

Figure 3. Crystallographically-derived solid-state structures of $\mathbf{6}^{iPr}$, $\mathbf{7}^{iPr}$ and $\mathbf{8}^{iPr}$. Atomic displacement ellipsoids drawn at 50% probability level. Ellipsoids on the ligand periphery and hydrogen atoms omitted for clarity, except for those involved in the C–H activation in $\mathbf{8}^{iPr}$.

The ^{11}B NMR shifts of $\mathbf{8}^{i\mathbf{Pr}}$ are significantly downfield-shifted from that of the iron 1,3,2,4-diazadiborolyl complex (δ_{11B} = 13.6 ppm),[20c] but are closer to those of η^5-1,2-azaborolyl iron complexes (δ_{11B} = 19–22 ppm).[21] Unfortunately, the formation of other minor byproducts (ca. 25%), the instability of $\mathbf{7}^{i\mathbf{Pr}}$ in solution and the similar crystallization rates of $\mathbf{7}^{i\mathbf{Pr}}$ and $\mathbf{8}^{i\mathbf{Pr}}$ prevented their clean isolation for further analyses.

*Reaction with di-*tert*-butylcarbodiimide*

In contrast, **II** reacted rapidly at room temperature with two equivalents of di-*tert*-butylcarbodiimide, independent of the stoichiometry used, to yield the isonitrile-stabilized FeBNC metallacycle $\mathbf{9}^{t\mathbf{Bu}}$, which shows an ^{11}B NMR shift at 66.3 ppm, similar to its phosphine-stabilized analogue $\mathbf{1}^{t\mathbf{Bu}}$ (δ_{11B} = 65.7 ppm). The byproduct of this reaction was the linear amino (imino)borane *t*BuN≡BN(SiMe$_3$)$_2$, compound $\mathbf{10}^{t\mathbf{Bu}}$ (δ_{11B} = 4.5 ppm, Scheme 4c), the ^{11}B NMR shift of which is comparable to that of *t*BuN≡BN(SiMe$_3$)*t*Bu (δ_{11B} = 3.0 ppm).[22] Fractional crystallization yielded a few crystals of complex $\mathbf{9}^{t\mathbf{Bu}}$ co-crystallized with the iminoborane dimer $\mathbf{11}^{t\mathbf{Bu}}$ (see Figure S48 in the Supporting Information) but its rapid decomposition in solution prevented its isolation in sufficient quantity for further analysis. Heating the mixture of $\mathbf{9}^{t\mathbf{Bu}}$ and $\mathbf{10}^{t\mathbf{Bu}}$ at 80 °C for several hours resulted in the formation of the iminoborane dimers (*t*BuNBR)$_2$ (R=Dur $\mathbf{3}^{t\mathbf{Bu}}$, N(SiMe$_3$)$_2$ $\mathbf{11}^{t\mathbf{Bu}}$, see solid-state structures in Figure S49 and Figure S51 in the Supporting Information), identified by their ^{11}B NMR shifts at 44.2 and 35.4 ppm, respectively. The latter is comparable to the related iminoborane (*t*BuNBN(SiMe$_3$)*t*Bu)$_2$ at 36.1 ppm.[23] The third product of this thermolysis was the known bis(isonitrile) iron complex $\mathbf{12}^{t\mathbf{Bu}}$,[24] which was repeatedly isolated as colorless crystals from the reaction mixture.

Reaction with bis(trimethylsilyl)carbodiimide

In a similar way to the reaction with **I**, the addition of bis(trimethylsilyl)carbodiimide to the bis(borylene) complex **II** led directly to the formation of all three possible iminoborane dimers, the symmetrical 1,3,2,4-diazadiboretidines (Me$_3$SiNBR)$_2$ (R=Dur $\mathbf{3}^{\mathbf{SiMe3}}$, N(SiMe$_3$)$_2$ $\mathbf{11}^{\mathbf{SiMe3}}$) and the unsymmetrical compound $\mathbf{13}^{\mathbf{SiMe3}}$ resulting from the cycloaddition of [Me$_3$SiN≡BN(SiMe$_3$)$_2$] and [Me$_3$SiN≡BDur]. These were identified by both their ^{11}B NMR shifts at 46.5, 27.0 and 38.0 ppm, respectively, as well as single-crystal X-ray crystallographic analyses of literature-known $\mathbf{11}^{\mathbf{SiMe3}}$,[25] and $\mathbf{13}^{\mathbf{SiMe3}}$ (see Figure S52 in the Supporting Information).

Postulated reaction mechanisms

Based on the reactivity of carbodiimides with the iron borylene complex **I**, it is possible to postulate a mechanism for the formation of $\mathbf{6}^{\mathbf{R}}$ (Scheme 5). Initially, DIC or DCC undergo a cycloaddition reaction with one of the two Fe=B moieties of **II**, yielding intermediate **Int1** (step i), which is analogous to $\mathbf{1}^{\mathbf{R}}$. This is followed by a cycloreversion step, which forms the iron isonitrile complex [Fe=BR′(C≡NR)(CO)$_3$] (**Int2**) and the linear iminoborane [RN≡BR′′] (**Int3**, step ii).[7] The latter undergoes a cycloaddition with the remaining Fe=BR′ borylene fragment of **Int2** to yield $\mathbf{6}^{\mathbf{R}}$ (step iii). The formation of $\mathbf{7}^{\mathbf{R}}$ upon heating can be rationalized as resulting from the insertion of the isonitrile carbon atom into the Fe–B$_{Dur}$ bond of $\mathbf{6}^{\mathbf{R}}$ (step iv), followed by sequential Fe–B bond cleavage and B–N bond formation (steps v and vi) in an analogous manner to steps i and ii in Scheme 3, generating the 1,3,2,4-diazadiborol-5-ylidene ligand. Although the subsequent mechanism of formation of $\mathbf{8}^{i\mathbf{Pr}}$ could not be probed, we suggest that the strained iron-bound carbon center in $\mathbf{7}^{i\mathbf{Pr}}$ is sufficiently basic to deprotonate an *i*Pr-methyl group and generate the bicyclic (diorganyl)iron(II) complex **Int6** (step vii), followed by insertion of a CO ligand into the Fe–C bond of the pendant 3-*N*-butanoyl ligand and cleavage of the Fe–C bond to the 5*H*-1,3,2,4-diazadiborol-5-yl ligand to form the half-

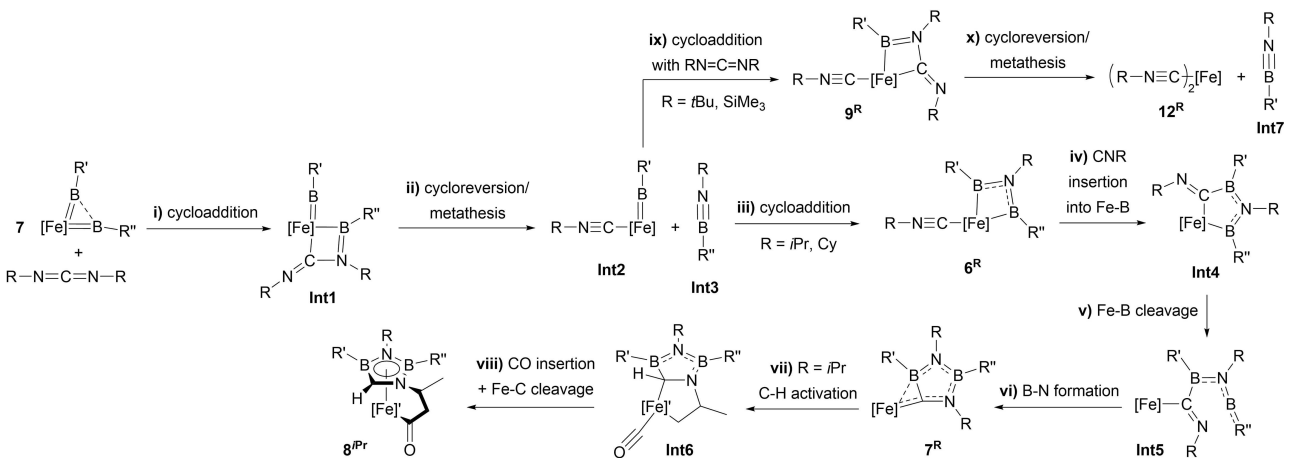

Scheme 5. Postulated mechanism for the formation of $\mathbf{6}^{\mathbf{R}}$–$\mathbf{9}^{\mathbf{R}}$. [Fe]=Fe(CO)$_3$; [Fe]′=Fe(CO)$_2$; R′=Dur; R′′=N(SiMe$_3$)$_2$.

sandwich complex **8**^{iPr} (step viii). The last step of thermally-induced CO insertion into Fe–C_{alkyl} bonds is well documented in iron(II) carbonyl chemistry and used in catalytic carbonylation reactions.[26] In the case of **7**^{Cy} the lower acidity of the cyclohexyl CH_2 protons prevents such C–H activation. With di-*tert*-butylcarbodiimide the formation of complex **9**^{tBu} can be rationalized by an initial metathesis process at the aminoborylene fragment (steps i and ii), after which the remaining iron isonitrile durylborylene **Int2** undergoes a cycloaddition reaction with another equivalent of di-*tert*-butylcarbodiimide to yield **9**^{tBu} (step ix), as the cycloaddition with the iminoborane **Int3** is prevented by the steric repulsion between the Dur and *t*Bu residues. Finally, with the more sterically encumbered di-*tert*-butyl- and bis(trimethylsilyl)carbodiimides steps i, ii and ix are followed by sterically-induced cycloreversion of **9**^{R} to yield the final metathesis products, the iron bis(isonitrile) complex **12**^{R} and the iminoborane [RNBDur] (**Int7**, step x), which dimerizes to **11**^{R}. The higher kinetic stability of the trimethylsilyl derivatives of the iminoborane monomers **Int3** and **Int7** allows both for homo- and cross-dimerization to occur, giving rise to the observed mixture of three 1,3,2,4-diazadiboretanes.

X-ray crystallographic analyses

Complexes 1^{R} and 9^{tBu}

The solid-state structures of **1**^{tBu}, **1**^{Tol}, **9**^{tBu} (see solid-state structures in Figures S38, S39 and S48 in the Supporting Information and structural parameters in Table 1) and **1**^{Cy} (Figure 2, Table 1) confirm the formation of the FeBNC ring. Interestingly, **9**^{tBu} co-crystallized with the dimer of the iminoborane byproduct, compound **11**^{tBu}. For **1**^{R} the iron center displays a distorted octahedral geometry, with the phosphine ligand and the endocyclic carbon atom C4 in axial positions (avg. P1–Fe1–C4 163.5°) and the boron atom B1 and the three CO ligands occupying the equatorial positions (avg. B1–Fe1–C3 167.4°; avg. C1–Fe1–C2 166.5°). For **9**^{tBu} one CO ligand occupies the axial position *trans* to C4 (C1–Fe1–C4 163.06(6)°), two occupy equatorial positions, one *trans* to B1 (B1–Fe1–C3 167.01(10)°), the other *cis* (B1–Fe1–C2 84.58(8)°), while the other equatorial position *cis* to B1 is occupied by the *tert*-butylisonitrile ligand (B1–Fe1–C5 87.53(8)°). The Fe–B bond length in **1**^{R} and **9**^{tBu} (avg. 2.13 Å) is significantly longer than in borylene **I** (1.7929(13) Å) and slightly longer than that observed in the related octahedral iron carbonyl boryl complex [Fe(BClDur)($SiMe_3$)(CO)$_3$(PMe_3)] (2.036(2) Å).[15] The strong *trans* influence of the boryl ligand[27] causes a slight elongation of the Fe1–C3 bond (avg. 1.81 Å) compared to the other two Fe–C_{CO} bonds (avg. 1.78 Å). The bond lengths within the metallacycle are indicative of a B1–N1 partial double bond (avg. 1.41 Å)[28] and N1–C4 (avg. 1.42 Å) and C4–Fe1 (avg. 2.04 Å) single bonds, while the exocyclic C4–N2 bond (avg. 1.26 Å) is clearly a double bond. For **9**^{tBu} the Fe1–C5 bond to the isonitrile ligand (1.8849(18) Å) is intermediate between the Fe1–C4 single bond (2.0749(17) Å) and the partial double bonds to the CO ligands (avg. 1.80 Å), suggesting some degree of π backbonding, albeit less than to the CO ligands. The only other crystallographically characterized MBNC metallacycle reported to date is the cycloaddition product of [CpMn=B*t*Bu(CO)$_2$] and DCC, which shows similar bonding.[5]

Complexes 2^{R}

The solid-state structures of **2**^{iPr} (see Figure S41 in the Supporting Information) and **2**^{Cy} (Figure 2, Table 1) confirm the insertion of carbodiimide units into both the Fe=B and B–C_{Dur} bonds. The iron center displays a slightly distorted trigonal bipyramidal geometry, with the phosphine and the C4 atom of the first inserted carbodiimide unit in the axial positions (avg. P1–Fe1–C4 170.6°) and the three CO ligands in the equatorial plane. The structural parameters of the boron bis(amidinate) moiety are very similar to that of analogous complexes

Table 1. Selected bond lengths (Å) and angles (°) for the solid-state structures of **1**^{tBu}, **1**^{Tol}, **1**^{Cy}, **9**^{tBu}, **2**^{iPr} and **2**^{Cy}.

	1^{tBu}	**1**^{Tol}[a]	**1**^{Cy}	**9**^{tBu}	**2**^{iPr}	**2**^{Cy}
Fe1–B1	2.1366(15)	2.1298(19), 2.1120(19)	2.150(3)	2.106(2)	–	–
B1–N1	1.4009(18)	1.410(2), 1.419(2)	1.397(3)	1.405(2)	1.535(4)	1.528(4)
N1–C4	1.4323(16)	1.413(2), 1.422(2)	1.428(3)	1.427(2)	1.359(4)	1.360(4)
C4–Fe1	2.0771(13)	2.0264(17), 2.0221(17)	2.036(2)	2.0749(17)	1.952(3)	1.948(3)
C4–N2	1.2548(17)	1.266(2), 1.268(2)	1.260(3)	1.259(2)	1.367(4)	1.361(4)
Fe1–X	2.2460(5)[b]	2.2457(8), 2.2477(7)[b]	2.2329(10)[b]	1.8849(18)[c]	2.1885(11)[b]	2.1966(9)[b]
Fe1–C1	1.7914(15)	1.7913(18), 1.7779(19)	1.780(2)	1.8064(19)	1.772(4)	1.766(4)
Fe1–C2	1.7796(15)	1.7840(19), 1.789(2)	1.782(2)	1.7758(19)	1.767(4)	1.764(4)
Fe1–C3	1.7991(14)	1.8119(19), 1.8138(19)	1.800(3)	1.8229(19)	1.778(3)	1.766(3)
B1–N2	–	–	–	–	1.517(5)	1.522(4)
B1–N3	–	–	–	–	1.587(5)	1.573(5)
B1–N4	–	–	–	–	1.577(5)	1.579(4)
C5–N3	–	–	–	–	1.332(4)	1.335(4)
C5–N4	–	–	–	–	1.327(4)	1.327(5)
B1–Fe1–C4	63.77(5)	64.43(7), 63.86(7)	63.90(10)	64.17(7)	–	–
X–Fe1–C4	161.26(4)[b]	160.33(5), 169.38(8)[b]	163.06(6)[b]	81.34(7)[c]	171.49(10)[b]	169.78(10)[b]
B1–Fe1–C3	169.66(6)	168.49(8), 164.31(8)	167.01(10)	173.73(8)	–	–
C1–Fe1–C2	166.43(6)	167.35(8), 167.77(5)	164.55(10)	98.49(8)	126.68(17)	129.05(16)

[a] Two distinct molecular units of **1**^{Tol} in the asymmetric unit. [b] X=P1. [c] X=C5.

Table 2. Selected bond lengths (Å) and angles (°) for the solid-state structures of 6^{iPr}, 6^{Cy}, 7^{iPr}, 7^{Cy} and 8^{iPr}.

	6^{iPr}	6^{Cy}	7^{iPr} [a]	7^{Cy}	8^{iPr}
Fe1–C4	1.8806(17)	1.875(3)	1.754(2), 1.760(2)	1.750(2)	–
Fe1–B1	2.1315(17)	2.125(3)	2.433(2), 2.448(2)	2.427(3)	–
C4–B1	–	–	1.621(3), 1.617(3)	1.609(4)	1.537(3)
B1–N1	1.414(2)	1.412(3)	1.433(3), 1.430(3)	1.432(3)	1.459(3)
N1–B2	1.448(2)	1.444(3)	1.453(3), 1.449(3)	1.451(4)	1.479(2)
B2–N2	1.430(2)	1.430(3)	1.445(3), 1.442(3)	1.460(4)	1.448(3)
B2–N3	–	–	1.466(3), 1.472(3)	1.450(3)	1.465(3)
N3–C4	–	–	1.347(3), 1.344(3)	1.352(3)	1.417(2)
B2–Fe1	2.1318(18)	2.141(3)	–	–	–
Fe1–C1	1.7800(17)	1.760(3)	1.759(2), 1.752(2)	1.753(3)	1.934(2)
Fe1–C2	1.7672(17)	1.778(3)	1.776(2), 1.774(2)	1.765(3)	1.777(2)
Fe1–C3	1.7995(17)	1.787(3)	1.826(2), 1.828(2)	1.830(3)	1.751(2)
C1–O1	1.155(2)	1.159(3)	1.149(3), 1.143(3)	1.153(3)	1.202(3)
C3–Fe1–C4	97.62(7)	98.93(11)	151.95(10), 152.62(9)	151.58(11)	–
C1–Fe1–C2	154.36(8)	157.10(11)	107.61(10), 107.93(10)	105.59(12)	–
B1–Fe1–C3	173.46(7)	173.10(11)	–	–	–
B2–Fe1–C4	149.35(7)	147.48(11)	–	–	–
Fe1–C4–N3	–	–	159.74(16), 159.03(16)	159.6(2)	–
Fe1–C4–B1	–	–	92.18(13), 92.84(13)	92.45(15)	–
(C3–Fe1–C4–B1)	–	–	−4.5(3), −3.9(3)	12.8(3)	–
(C4–Fe1–B1–N1)	−175.4(1)	−178.8(2)	–	–	–
Fe1···(CB_2N_2 plane)	–	–	–	–	ca. 1.81

[a] Two distinct molecular units of 7^{iPr} in the asymmetric unit.

obtained from the double insertion of DCC or DIC into $[CpFe{=}B{=}NCy_2(CO)_2]^+$,[8c] with delocalized π bonding over both N–C–N units (avg. N–C 1.35 Å). The Fe1–P1 (avg. 2.19 Å) and Fe1–C4 (avg. 1.95 Å) bond lengths are also comparable to those of *trans*-$[Fe(IMes)(PMe_3)(CO)_3]$ (Fe–P 2.1980(8), Fe–C_{IMes} 1.984(2) Å),[17] thus reinforcing the hypothesis of the carbenoid character of the 1,3,4-diazaboretidin-2-yl moiety.

Complexes 6^R

The solid-state structures of 6^{iPr} (Figure 3, Table 2) and 6^{Cy} (see Figure S44 in the Supporting Information) confirm the formation of the FeBNB heterocycle. Complexes 6^R present a much more strongly distorted octahedral geometry than 1^R and 9^{tBu}. The axial positions are occupied by the diaminoboryl ligand moiety and the isonitrile ligand (avg. C4–Fe1–B2 148.4°) and the equatorial positions by the amino(duryl)boryl moiety and three CO ligands. The strong *trans* influence of the boryl ligand is apparent in the slight elongation of the Fe1–C3 bond (avg. 1.79 Å) compared the other two Fe–C_{CO} bonds (avg. 1.77 Å). The Fe1–C4 bond to the isonitrile ligand (avg. 1.88 Å) is similar to that is complex 9^{tBu} (1.8849(18) Å). Furthermore, the isonitrile ligand is nearly coplanar with the FeBNB metallacycle as seen by the (C4–Fe1–B1–N1) torsion angle (avg. −177.1°) approaching 180°. The two Fe–B bond lengths (avg. 2.13 Å) are similar to each other and to those in 1^R and 9^{tBu} (avg. 2.13 Å). The B–N bond lengths (avg. 1.43 Å) indicate π delocalization over B1–N1–B2–N2. Complexes 6^R are only the second crystallographically characterized examples of *cis*-diboryl iron complexes, the first being the tetrahedral FeB_4 metallacycle, $[Fe\{B(Dur)BN(SiMe_3)_2\}_2(CO)_2]$ obtained by irradiating **II** followed by heating at 80 °C under a CO atmosphere.[11]

Complexes 7^R

The solid-state structures of 7^{iPr} (Figure 3, Table 2) and 7^{Cy} (see Figure S46 in the Supporting Information) confirm the formation of a unique aromatic 1,3,2,4-diazadiborol-5-ylidene ligand. The iron center adopts a rare, highly distorted seesaw geometry, with the carbon atom of the CB_2N_2 heterocycle and one CO ligand in axial positions (avg. C3–Fe1–C4 152.1°) and the other two CO ligands in *cis*-equatorial positions (avg. C1–Fe1–C2 107.0°). There are only a couple of seesaw iron complexes described in the literature, in which this unusual geometry is enforced by bidentate ligands with a very wide bite angle.[29] The seesaw geometry in 7^R is enforced by a weak interaction between the electron-rich iron center and the electron-poor duryl-substituted boron atom B1 (avg. Fe1···B1 2.44 Å). This interaction also causes the CB_2N_2 heterocycle to tilt towards the iron center, thereby imposing a very strained geometry at C4, with the Fe1–C1–N2 angle tending towards linearity (avg. 159.5°) and the Fe1–C4–B1 angle towards orthogonality (avg. 92.5°). Such Fe···B interactions have been observed in boryl- and borolyl-substituted ferrocenes, in which they cause the boron substituent to tilt towards the iron center.[30] The Fe···B distance in these complexes (2.66–3.00 Å)[30] is significantly longer than in 7^R (2.44 Å). The Fe1–C4 bond in 7^R (avg. 1.75 Å) is of similar length to the equatorial Fe–C_{CO} bonds (avg. 1.76 Å), thereby indicating a significant amount of π bonding between Fe1 and C4. It is thus likely that the 1,3,2,4-diazadiborol-5-ylidene ligand has carbenoid character, as shown in Figure 4.

The Fe1–C3 bond to the axial CO in 7^R (avg. 1.83 Å) is longer than the equatorial Fe–C_{CO} bonds and the Fe–C_{CO} bonds *trans* to the boryl substituents in 1^R (avg. 1.81 Å), suggesting that the 1,3,2,4-diazadiborol-5-ylidene ligand has a very strong *trans* influence. Furthermore, the axial CO ligand is nearly coplanar

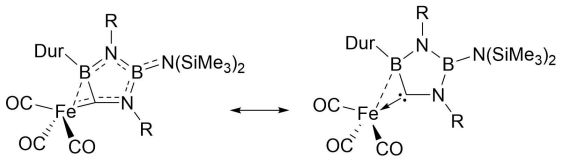

Figure 4. Resonance structures of $\mathbf{7^R}$ highlighting the carbenoid character of the 1,3,2,4-diazadiborol-5-ylidene ligand.

with the CB_2N_2 heterocycle (avg. torsion angle |C3–Fe1–C4–B1| 7.1°) and positioned just underneath and parallel to the duryl substituent ($C1\cdots Dur_{plane}$ ca. 2.90 Å), presumably in order to maximize π overlap. Whereas the endocyclic C4–B1 bond (avg. 1.66 Å) is a single bond, the other endocyclic bonds (avg. B1–N1 1.43, N1–B2 1.45, B2–N3 1.46, N3–C4 1.35 Å) are all within the range of partial double bonds, indicating a π delocalized B1–N1–B2–N3–C4–Fe1 framework.

Complex 8^{iPr}

The solid-state structure of $\mathbf{8^{iPr}}$ (Figure 3, Table 2) shows an iron (II) piano-stool motif with a unique η^5-1,3,2,4-diazadiborolyl ligand tethered to the iron center by a 3-*N*-butanoyl side arm, the coordination sphere being completed by two CO ligands. The distance from the iron center to the CB_2N_2 plane is ca. 1.81 Å, which is slightly longer than in the analogous iron cyclopentadienyl piano-stool complex [{η^1-C(=O)CH_2CH_2–(η^5-C_5H_4)}Fe$(CO)_2$] (ca. 1.73 Å), in which the Cp ligand is similarly tethered to the iron center via a 3-*N*-propanoyl side arm.[31] Conversely, the Fe1–C1 bond to the acyl ligand (1.934(2) Å) is slightly shorter than in the above-mentioned iron cyclopentadienyl complex (1.978(2) Å). The endocyclic bond lengths of the CB_2N_2 heterocycle (C4–B1 1.537(3), B1–N1 1.459(3), N1–B2 1.479(2), B2–N3 1.465(3), N3–C4 1.417(2) Å) are all within the range of partial double bonds, indicating full π delocalization and an aromatic character.

Conclusion

Although the reactions of the iron durylborylene complex **I** and the iron bis(borylene) complex **II** with carbodiimides yield a plethora of products, dependent upon the carbodiimide substituents, it is possible to rationalize these via a series of simple cycloaddition, metathesis, rearrangement, and insertion steps, which seem mainly dictated by steric factors. While the FeBNC-metallacylic cycloaddition products $\mathbf{1^R}$, from reactions between **I** and carbodiimides, are isolable with all but the most sterically hindered carbodiimides (R=Tol, *i*Pr, Cy, *t*Bu), they are not thermally stable and undergo cycloreversion to the corresponding metathesis products, the dimeric iminoboranes $\mathbf{3^R}$ and iron isonitrile complexes $\mathbf{4^R}$, as well as the iron carbene complexes $\mathbf{5^R}$, which result from the rearrangement of $\mathbf{1^R}$. For the less sterically hindered carbodiimides (R = *i*Pr, Cy), $\mathbf{5^R}$ can undergo the insertion of a second equivalent of carbodiimide into the B–C_{Dur} bond to yield iron complexes bearing a *spiro*-boracarbene ligand, $\mathbf{2^R}$. Similar reactivity patterns can be observed for the bis(borylene) complex **II**, in which metathesis/cycloaddition sequences either yield the novel isonitrile-bound FeBNB-metallacycles $\mathbf{6^R}$ for the least sterically hindered carbodiimides (R = *i*Pr, Cy) or the unstable isonitrile-bound FeBNC metallacycle $\mathbf{9^R}$ for the more sterically demanding *t*Bu derivative. Heating $\mathbf{6^R}$ leads to the insertion of both the C and N atoms of the isonitrile ligand into the Fe–B bonds, forming unprecedented 1,3,2,4-diazadiborol-5-ylidene complexes, $\mathbf{7^R}$. The $\mathbf{7^{iPr}}$ derivative undergoes a C–H activation and CO insertion at an *iso*propyl group to yield a 1,3,2,4-diazadiborolyl pianostool complex tethered by an acyl side arm, complex $\mathbf{8^{iPr}}$. For the most sterically demanding bis(trimethylsilyl)carbodiimide derivative the only products observed in either case are the final metathesis products, as the cycloaddition intermediates are all kinetically unstable. While the complex product mixtures of these reactions and their instability often prevented the clean isolation of the compounds of interest, this study highlights the potential of transition metal borylene complexes for the synthesis of novel B,N-metallacycles and highly electron-donating B,N-heterocyclic analogues of common organic ligands, such as carbenes or cyclopentadienyls.

Experimental Section

Methods and materials. All manipulations were performed either under an atmosphere of dry argon or *in vacuo* using standard Schlenk line or glovebox techniques. Deuterated solvents were dried over molecular sieves and degassed by three freeze-pump-thaw cycles prior to use. All other solvents were distilled and degassed from appropriate drying agents. Both deuterated and non-deuterated solvents were stored under argon over activated 4 Å molecular sieves. NMR spectra were acquired either on a Bruker Avance 500 or a Bruker Avance 400 NMR spectrometer. Chemical shifts (δ) are provided in ppm and internally referenced to the carbon nuclei ($^{13}C\{^1H\}$) or residual protons (^1H) of the solvent. Heteronuclear NMR spectra are referenced to external standards (^{11}B: $BF_3{\bullet}OEt_2$; ^{31}P: 85% H_3PO_4 in H_2O). NMR multiplicities are given as: s (singlet), d (doublet), m (multiplet), br (broad). The multiplicity of $^{13}C\{^1H\}$ NMR resonances is s, unless specified otherwise. Solid-state IR spectra were recorded on a Bruker FT-IR spectrometer ALPHA II inside a glovebox. Microanalyses (C, H, N, S) were performed on an Elementar vario MICRO cube elemental analyzer. Carbodiimides were purchased from Sigma-Aldrich or Alfa Aesar and used as received. Complexes **I**[6] and **II**[11] were synthesized using literature procedures.

The crystal data of $\mathbf{1^R}$ (R=Cy, *t*Bu, Tol), $\mathbf{2^R}$ (R = *i*Pr, Cy), $\mathbf{3^{tBu}}$, $\mathbf{6^R}$ (R = *i*Pr, Cy), $\mathbf{7^R}$ (R = *i*Pr, Cy) and $\mathbf{11^{tBu}}$ were collected on a Bruker X8-APEX II diffractometer with a CCD area detector and multi-layer mirror monochromated $Mo_{K\alpha}$ radiation. The crystal data of $\mathbf{3^{SiMe3}}$, $\mathbf{8^{iPr}}$, $\mathbf{9^{tBu}}{\cdot}\mathbf{11^{tBu}}$ and $\mathbf{13^{SiMe3}}$ were collected on a Bruker D8 Quest diffractometer with a CMOS area detector and multi-layer mirror monochromated $Mo_{K\alpha}$ radiation. The structures were solved using the intrinsic phasing method,[32] refined with the ShelXL program[33] (see Supporting Information for refinement details) and expanded using Fourier techniques. All non-hydrogen atoms were refined anisotropically. Hydrogen atoms were included in structure factor calculations. All hydrogen atoms were assigned to idealized geometric positions, except for those bound to N2, which were detected in the inverse Fourier map and refined freely. Crystallo-

graphic data have been deposited with the Cambridge Crystallographic Data Center.

Synthesis of 1^{tBu}. 100 mg (278 μmol) of **I** were dissolved in hexane (10 mL) and 42.8 mg (53.5 μL, 278 μmol) di-*tert*-butylcarbodiimide were added. After stirring the reaction mixture at rt overnight all volatiles were removed in vacuo, after which the solid residue was extracted with 10 mL of hexane. Partial removal of the solvent in vacuo yielded a colorless crystalline solid, which was washed with pentane, affording $\mathbf{1}^{tBu}$ in 48% yield (68.0 mg 132 μmol). ^{1}H NMR (400.1 MHz, C_6D_6): $\delta = 0.60$ (d, 9H, $^2J_{PH} = 8.8$ Hz, P(CH_3)$_3$), 1.63 (s, 9H, C(CH_3)$_3$), 1.68 (s, 9H, C(CH_3)$_3$), 2.05 (s, 6H, Dur–CH_3), 2.36 (s, 6H, Dur–CH_3), 6.75 (s, 1H, Dur–CH) ppm. ^{13}C{^{1}H} NMR (100.6 MHz, C_6D_6): $\delta = 18.7$ (d, $^1J_{PC} = 27.6$ Hz, P(CH_3)$_3$), 19.7 (Dur–CH_3), 21.1 (Dur–CH_3), 30.2 (C(CH_3)$_3$), 30.6 (C(CH_3)$_3$), 53.5 (d, $^4J_{PC} = 1.4$ Hz, C(CH_3)$_3$), 61.8 (d, $^4J_{PC} = 0.8$ Hz, C(CH_3)$_3$), 130.8 (Dur–CH), 132.7 (*m*-Dur–*C*), 133.8 (*o*-Dur–*C*), 147.0 (*i*-Dur–C, detected by HMBC), 154.5 (d, $^2J_{PC} = 10.5$ Hz, Fe*C*), 214.1 (br, CO), 216.4 (br, *C*O) ppm. ^{11}B NMR (128.4 MHz, C_6D_6): $\delta = 65.7$ (br) ppm. ^{31}P{^{1}H} NMR (162.0 MHz, C_6D_6): $\delta = 9.1$ (s) ppm. FT-IR (solid-state): $\tilde{\nu}$(CO) = 2022, 1954, 1936 cm^{-1}. Elemental analysis (%) calcd. for $C_{15}H_{27}FeBPO_3N_2$: C 58.39, H 7.84 N 5.45; found: C 58.06, H 7.58, N 5.22.

Synthesis of 1^{Tol}. 100 mg (278 μmol) of **I** and 61.8 mg (278 μmol) of di-*p*-tolylcarbodiimide were dissolved in 10 mL of a 1:1 hexane/toluene mixture. After stirring the reaction mixture at rt overnight all volatiles were removed in vacuo, after which the solid residue was washed with 10 mL of hexane, affording $\mathbf{1}^{Tol}$ as a colorless solid in 57% yield (92.2 mg 158 μmol). ^{1}H NMR (400.1 MHz, CD_2Cl_2): $\delta =$ 1.10 (d, 9H, $^2J_{PH} = 9.1$ Hz, P(CH_3)$_3$), 2.14 (s, 6H, Dur–CH_3), 2.25 (s, 9H, Dur + Tol–CH_3), 2.30 (s, 3H, Tol–CH_3), 6.71 (d, 2H, $^3J = 8.0$ Hz, Tol–CH), 6.86 (s, 1H, Dur–CH), 7.04 (d, 2H, $^3J = 7.8$ Hz, Tol–CH), 7.11 (d, 2H, $^3J = 7.8$ Hz, Tol–CH), 7.23 (d, 2H, $^3J = 8.0$ Hz, Tol–CH) ppm. ^{13}C{^{1}H} NMR (100.6 MHz, CD_2Cl_2): $\delta = 19.3$ (d, $^1J_{PC} = 29.2$ Hz, P(CH_3)$_3$), 19.7 (Dur–CH_3), 20.3 (Dur–CH_3), 20.9 (Tol–CH_3), 21.1 (Dur–CH_3), 121.9 (Tol–*C*H), 124.7 (Tol–*C*H), 129.3 (Tol–*C*H), 129.7 (Tol–*C*H), 131.7 (Dur–*C*H), 132.1 (*p*-Tol–*C*), 133.5 (*m*-Dur–*C*), 134.1 (*o*-Dur–*C*), 135.6 (*p*-Tol–*C*), 139.5 (d, $^4J_{PC} = 1.7$ Hz, *i*-Tol–*C*), 142.3 (*i*-Dur–C, detected by HMBC), 151.6 (*i*-Tol–*C*), 169.0 (Fe*C*, detected by HMBC), 212.4 (br, *C*O), 214.6 (br, *C*O) ppm. ^{11}B NMR (128.4 MHz, CD_2Cl_2): $\delta =$ 69.3 (br) ppm. ^{31}P{^{1}H} NMR (162.0 MHz, CD_2Cl_2): $\delta = 11.5$ (s) ppm. FT-IR (solid-state): $\tilde{\nu}$(CO) = 2028, 1979, 1944 cm^{-1}. Elemental analysis (%) calcd. for [$C_{31}H_{36}BFeN_2O_3P$]: C 63.95, H 6.23, N 4.81; found.: C 63.20, H 6.63, N 4.30.

Synthesis of 1^{iPr} and 2^{iPr}. 50.0 mg (139 μmol) of **I** were dissolved in hexane (10 mL) and 17.5 mg (21.5 μL, 139 μmol) of DIC were added. The mixture was stirred at rt overnight, after which all volatiles were removed *in vacuo* and the solid residue extracted with 10 mL of hexane. Removal of all volatiles yielded an 87:13 mixture of $\mathbf{1}^{iPr}$ and $\mathbf{2}^{iPr}$ as determined by ^{1}H, ^{11}B and ^{31}P NMR-spectroscopic analysis. After storage of the solution at 30 °C overnight colorless single crystals of $\mathbf{1}^{iPr}$ suitable for X-ray diffraction analysis were obtained. The amount isolated for $\mathbf{1}^{iPr}$, however, was too small for full characterization. Multiple attempts to separate $\mathbf{1}^{iPr}$ and $\mathbf{2}^{iPr}$ by fractional crystallization failed, which is why only ^{1}H, ^{11}B and ^{31}P NMR data of the mixture were collected. **NMR data for 1^{iPr}:** ^{1}H NMR (400.1 MHz, C_6D_6): $\delta = 0.67$ (d, $^2J_{PH} = 9$H, P(CH_3)$_3$), 1.34 (d, 6H, $^3J =$ 6.7 Hz, CH(CH_3)$_2$), 1.54 (d, 6H, $^3J = 6.3$ Hz, CH(CH_3)$_2$), 2.06 (s, 6H, Dur–CH_3), 2.35 (s, 6H, Dur–CH_3), 3.83 (sept, $^3J = 6.3$ Hz, 1H, CH(CH_3)$_2$), 4.68 (sept, $^3J = 6.7$ Hz, 1H, CH(CH_3)$_2$), 6.80 (s, 1H, Dur–CH)ppm. ^{11}B NMR (128.4 MHz, C_6D_6): $\delta = 63.2$ (br) ppm. ^{31}P NMR (162.0 MHz, C_6D_6): $\delta = 10.2$ (s) ppm. **NMR data for 2^{iPr}:** ^{1}H NMR (400.1 MHz, C_6D_6): $\delta = 1.05$ (d, $^3J = 6.4$ Hz, 12H, CH(CH_3)$_2$), 1.44 (d, $^2J_{PH} = 9.1$ Hz, 9H, P(CH_3)$_3$), 1.53 (d, $^3J = 6.5$ Hz, 12H, CH(CH_3)$_2$), 1.89 (s, 6H, Dur–CH_3), 1.97 (s, 6H, Dur–CH_3), 3.27 (sept, $^3J = 6.5$ Hz, 2H, CH(CH_3)$_2$), 3.34 (sept, $^3J = 6.4$ Hz, 2H, CH(CH_3)$_2$), 6.74 (s, 1H, Dur–CH)ppm. ^{11}B NMR (128.4 MHz, C_6D_6): $\delta = 6.6$ (s) ppm. ^{31}P NMR (162.0 MHz, C_6D_6): $\delta = 39.3$ (s) ppm.

Synthesis of 1^{Cy} and 2^{Cy}. 50.0 mg (139 μmol) of **I** were dissolved in hexane (10 mL) and 17.5 mg (139 μmol) of DCC were added. The mixture was stirred at rt overnight, after which all volatiles were removed *in vacuo* and the solid residue extracted with 10 mL of hexane. Removal of all volatiles yielded an 75:25 mixture of $\mathbf{1}^{Cy}$ and $\mathbf{2}^{Cy}$ as determined by ^{11}B and ^{31}P NMR-spectroscopic analysis. Fractional crystallization at 30 °C afforded colorless single crystals of $\mathbf{1}^{Cy}$ and $\mathbf{2}^{Cy}$ suitable for X-ray diffraction analysis. The amount isolated for $\mathbf{1}^{Cy}$, however, was too small for full characterization, which is why only ^{1}H, ^{11}B and ^{31}P NMR data were collected. Multiple attempts to separate $\mathbf{2}^{Cy}$ by fractional crystallization failed, and only its ^{11}B and ^{31}P NMR data could be determined, as the ^{1}H NMR data $\mathbf{2}^{Cy}$ overlapped too much with that of $\mathbf{1}^{Cy}$ to extract it from the spectrum of the mixture. **NMR data for 1^{Cy}:** ^{1}H NMR (400.1 MHz, C_6D_6): $\delta = 0.67$ (d, 9H, $^2J_{PH} = 8.8$ Hz, P(CH_3)$_3$), 0.81–0.93 (m, 1H, Cy–CH_2), 1.11–1.21 (m, 2H, Cy–CH_2), 1.34–1.37 (m, 2H, Cy–CH_2), 1.52–1.56 (m, 2H, Cy–CH_2), 1.62–1.79 (m, 5H, Cy–CH_2), 1.86–1.95 (m, 4H, Cy–CH_2), 2.06 (s, 6H, Dur–CH_3), 2.17–2.24 (m, 4H, Cy–CH_2), 2.41 (s, 6H, Dur–CH_3), 3.51–3.64 (m, 1H, Cy–CH), 4.49–4.63 (m, 1H, Cy–CH), 6.78 (s, 1H, Dur–CH) ppm. ^{13}C{^{1}H} NMR (100.6 MHz, C_6D_6): $\delta = 18.9$ (d, $^1J_{PC} = 28.1$ Hz, P(CH_3)$_3$), 19.8 (Dur–CH_3), 21.2 (Dur–CH_3), 25.5 (Cy–CH_2), 26.1 (Cy–CH_2), 26.3 (Cy–CH_2), 26.7 (Cy–CH_2), 32.7 (Cy–CH_2), 35.5 (Cy–CH_2), 58.1 (Cy–CH), 63.3 (d, $^4J_{PC} = 2.4$ Hz, Cy–CH), 131.4 (Dur–*C*H), 133.5 (Dur–C_q), 133.8 (Dur–C_q), 143.8 (*i*-Dur–C, detected by HMBC), 158.2 (d, $^2J_{PC} = 10.2$ Hz, Fe*C*), 214.3 (br, *C*O), 215.8 (br, *C*O) ppm. ^{11}B NMR (128.4 MHz, C_6D_6): $\delta = 63.3$ (br) ppm. ^{31}P{^{1}H} NMR (162.0 MHz, C_6D_6): $\delta = 10.2$ (s) ppm. **NMR data for 2^{Cy}:** ^{11}B NMR (128.4 MHz, C_6D_6): $\delta = 6.9$ (s) ppm. ^{31}P{^{1}H} NMR (162.0 MHz, C_6D_6): $\delta = 39.6$ (s) ppm.

Thermolysis of 1^{iPr} and 2^{iPr}. A 87:13 mixture of $\mathbf{1}^{iPr}$ and $\mathbf{2}^{iPr}$ was heated in C_6D_6 for 3 days at 80 °C, resulting in ca. 90% conversion to a 51:39 mixture of the iron complexes $\mathbf{4}^{iPr}$ and $\mathbf{5}^{iPr}$, as determined by ^{11}B and ^{31}P NMR spectroscopy, and the iminoborane dimer $\mathbf{3}^{iPr}$, [DurB=N*i*Pr]$_2$, as determined by ^{11}B NMR spectroscopy. Fractional crystallization yielded colorless crystals of $\mathbf{3}^{iPr}$ suitable for X-ray crystallographic analysis. However, none of the products could be separated from the mixture in sufficient quantity and purity for further analyses. ^{11}B NMR (128.4 MHz, C_6D_6): $\delta = 41.5$ (v. br, $\mathbf{5}^{iPr}$), 44.0 (br, $\mathbf{3}^{iPr}$) ppm. ^{31}P{^{1}H} NMR (162.0 MHz, C_6D_6): $\delta = 37.7$ (br, $\mathbf{5}^{iPr}$), 38.3 (br, $\mathbf{4}^{iPr}$) ppm.

Thermolysis of 1^{Cy} and 2^{Cy}. A 75:25 mixture of $\mathbf{1}^{Cy}$ and $\mathbf{2}^{Cy}$ was heated in C_6D_6 for 3 days at 80 °C, resulting in ca. 85% conversion to a 50:35 mixture of the iron complexes $\mathbf{4}^{Cy}$ and $\mathbf{5}^{Cy}$, as determined by ^{11}B and ^{31}P NMR spectroscopy, and the iminoborane dimer $\mathbf{3}^{Cy}$, [DurB=NCy]$_2$, as determined by ^{11}B NMR spectroscopy. Fractional crystallization yielded colorless crystals of $\mathbf{3}^{Cy}$ suitable for X-ray crystallographic analysis. However, none of the products could be separated from the mixture in sufficient quantity and purity for further analyses. ^{11}B NMR (128.4 MHz, C_6D_6): $\delta = 44.6$ (v. br, $\mathbf{3}^{Cy} + \mathbf{5}^{Cy}$) ppm. ^{31}P{^{1}H} NMR (162.0 MHz, C_6D_6): $\delta = 38.1$ (br, $\mathbf{5}^{Cy}$), 38.6 (br, $\mathbf{4}^{Cy}$) ppm.

Reaction of I with bis(trimethylsilyl)carbodiimide. 10 mg (28 μmol) of **I** and 5.2 mg (6.3 μL, 28 μmol) of bis(trimethylsilyl) carbodiimide were combined in C_6D_6 (0.5 mL). After 10 min at rt ^{11}B NMR-spectroscopic analysis showed full conversion to a ca. 1:1 product mixture of $\mathbf{3}^{SiMe3}$ and $\mathbf{5}^{SiMe3}$. Recrystallization from hexane at −30 °C yielded colorless crystals of $\mathbf{3}^{SiMe3}$ suitable for X-ray diffraction analysis. None of the products could be isolated in sufficient purity for further analyses. ^{11}B NMR (128.4 MHz, C_6D_6): $\delta =$ 46.8 (br, $\mathbf{3}^{SiMe3}$), 37.4 (br, $\mathbf{5}^{SiMe3}$) ppm. ^{31}P NMR (162.0 MHz, C_6D_6): $\delta =$ 36.7 (br, $\mathbf{5}^{SiMe3}$), 37.1 (br, $\mathbf{4}^{SiMe3}$) ppm.

Synthesis of 6^{iPr}. 100 mg (220 μmol) of the bis(borylene) iron complex **II** were dissolved in hexane (20 mL) and 27.7 mg (34.0 μL, 220 μmol) of DIC were added. After 1 h stirring at rt all volatiles were removed *in vacuo* and the solid residue extracted with hexane (1 mL). Storage of the resulting solution at −30 °C yielded compound 6^{iPr} as a colorless crystalline solid in 58% yield (75.1 mg, 129 μmol). ^{1}H NMR (400.1 MHz, C_6D_6): $\delta = 0.48$ (d, 6H, $^3J = 6.63$ Hz, CH(CH_3)$_2$), 0.53 (s, 18H, Si(CH_3)$_2$), 1.15 (d, 6H, $^3J = 6.63$ Hz, CH(CH_3)$_2$), 2.12 (s, 6H, Dur–CH_3), 2.41 (s, 6H, Dur–CH_3), 2.82 (sept., 1H, $^3J = 6.63$ Hz, C*H*(CH$_3$)$_2$), 4.07 (sept., 1H, $^3J = 6.63$ Hz, C*H*(CH$_3$)$_2$) 6.81 (s, 1H, Dur–C*H*) ppm. ^{13}C{^{1}H} NMR (100.6 MHz, C_6D_6): $\delta = 4.5$ (Si(CH$_3$)$_3$), 19.9 (Dur–CH$_3$), 20.5 (Dur–CH$_3$), 22.4 (CH(CH$_3$)$_2$), 23.1 (CH(CH$_3$)$_2$), 47.9 (CH(CH$_3$)$_2$), 51.3 (CH(CH$_3$)$_2$), 130.6 (Dur–CH), 131.9 (*m*-Dur–*C*), 133.1 (*o*-Dur–*C*), 147.5 (br, *i*-Dur–*C*) 215.6 (CO) ppm. *Note: the iron-bound isonitrile carbon $^{13}C\{^1H\}$ NMR resonance could not be detected, even by HMBC.* ^{11}B NMR (128.4 MHz, C_6D_6): $\delta = 51.7$ (*B*N(SiMe$_3$)$_2$), 67.6 (*B*Dur) ppm. FT-IR (solid-state): $\tilde{\nu}$(CN) = 2163 cm^{-1}; $\tilde{\nu}$(CO) = 1997, 1936, 1912, 1885 cm^{-1}. *Note: the compound was too sensitive to obtain satisfactory elemental analysis data.*

Synthesis of 6^{Cy}. 100 mg (220 μmol) of the bis(borylene) iron complex **II** were dissolved in hexane (20 mL) and 45.3 mg (220 μmol) of DCC were added. After 1 h stirring at rt all volatiles were removed *in vacuo* and the solid residue extracted with hexane (1 mL). Storage of the resulting solution at −30 °C yielded compound 6^{Cy} as a colorless crystalline solid in 31% yield (45 mg, 68.0 μmol). ^{1}H NMR (400.1 MHz, C_6D_6): $\delta = 0.56$ (s, 18H, Si(CH_3)$_2$), 0.67–1.62 (m, 20H, Cy–CH_2), 2.13 (s, 6H, Dur–CH_3), 2.47 (s, 6H, Dur–CH_3), 2.62–2.75 (m, 1H, Cy–C*H*), 3.70–3.83 (m, 1H, Cy–C*H*), 6.79 (s, 1H, Dur–C*H*) ppm. ^{11}B NMR (128.4 MHz, C_6D_6): $\delta = 51.5$ (*B*N(SiMe$_3$)$_2$), 68.1 (*B*Dur) ppm. *Note: as 6^{Cy} slowly decomposed at room temperature in solution into 7^{Cy} and a number of minor unidentified byproducts no clean $^{13}C\{^1H\}$ NMR data could be recorded.* FT-IR (solid-state): $\tilde{\nu}$(CN) = 2148, 2130 cm^{-1}; $\tilde{\nu}$(CO) = 1999, 1942, 1922 cm^{-1}. *Note: the compound was too sensitive to obtain satisfactory elemental analysis data.*

Thermolysis of 6^{iPr}. 6^{iPr} was heated in C_6D_6 for 4 h at 80 °C, slowly turning dark red and resulting in ca. 75% conversion to a ca. 45:30 mixture of the iron complexes 7^{iPr} and 8^{iPr}, as determined by ^{11}B NMR spectroscopy. Fractional crystallization yielded red crystals of 7^{iPr} and orange crystals of 8^{iPr} suitable for X-ray crystallographic analyses. However, due to their similar crystallization properties and the presence of intractable byproducts, neither 7^{iPr} nor 8^{iPr} could be separated from the mixture in sufficient quantity and purity for further analyses. ^{11}B NMR (128.4 MHz, C_6D_6): δ = 45.0 (v. br, unknown byproduct), 41.1 (br, *B*Dur, 7^{iPr}), 33.1 (br, *B*N(SiMe$_3$)$_2$, 7^{iPr}), 29.6 (br, *B*Dur, 8^{iPr}), 21.0 (br, *B*N(SiMe$_3$)$_2$, 8^{iPr}) ppm.

Thermolysis of 6^{Cy}. 6^{Cy} was heated in C_6D_6 for 4 h at 80 °C, slowly turning dark red and resulting in ca. 80% conversion to the iron complex 7^{Cy}, as determined by ^{11}B NMR spectroscopy. Fractional crystallization yielded red crystals of 7^{Cy} suitable for X-ray crystallographic analysis. However, due to the presence of intractable byproducts 7^{Cy} could be separated from the mixture in sufficient quantity and purity for further analyses. ^{11}B NMR (128.4 MHz, C_6D_6): δ = 51.9 (v. br, unknown byproduct), 41.8 (br, *B*Dur, 7^{Cy}), 33.6 (br, *B*N(SiMe$_3$)$_2$, 7^{Cy}) ppm.

Synthesis of 9^{tBu} and 10^{tBu}. 20.0 mg (43.9 μmol) of **II** and 13.6 mg (17.0 μL, 88.2 μmol) of di-*tert*-butylcarbodiimide were combined in 0.5 mL of hexane. After 30 min at rt ^{11}B NMR-spectroscopic analysis showed full conversion to 9^{tBu} and 10^{tBu}. Colorless single crystals of a $9^{tBu}\cdot 11^{tBu}$ co-crystal suitable for X-ray diffraction analysis could be obtained by crystallization from hexane at −30 °C. However, the rapid decomposition of the product mixture at rt in solution prevented the acquisition of further analytical data. ^{11}B NMR (128.4 MHz, C_6D_6): δ = 66.3 (v. br, 9^{tBu}), 4.5 (br, 10^{tBu}) ppm.

Thermolysis of 9^{tBu} and 10^{tBu}. The mixture of 9^{tBu} and 10^{tBu} obtained above was heated for 4 h at 80 °C, leading to the formation of a 1:1 mixture of the iminoborane dimers 3^{tBu} and 11^{tBu}, as determined by ^{11}B NMR spectroscopy. Single crystals of both dimers suitable for X-ray crystallographic analyses were obtained from the hexane solution stored at −30 °C, as well as colorless crystals of the iron byproduct 12^{tBu}.[34] ^{11}B NMR (128.4 MHz, C_6D_6): $\delta = 44.6$ (br, 3^{tBu}), 35.4 (br, 11^{tBu}) ppm.

Reaction of II with bis(trimethylsilyl)carbodiimide. 20.0 mg (43.9 μmol) of **II** and 16.4 mg (20.0 μL, 88.1 μmol) of bis(trimethylsilyl)carbodiimide were combined in C_6D_6 (0.5 mL). After 10 min at rt ^{11}B NMR-spectroscopic analysis showed full conversion to a mixture of 3^{SiMe3}, 11^{SiMe3} and 13^{SiMe3}. Recrystallization from hexane at −30 °C yielded colorless crystals of all three dimers suitable for X-ray diffraction analysis (the structure of 11^{SiMe3} is literature-known).[25] None of the products could be isolated in sufficient purity for further analyses. ^{11}B NMR (128.4 MHz, C_6D_6): δ = 46.5 (br, 3^{SiMe3}), 37.4 (br, 13^{SiMe3}), 27.0 (br, 11^{SiMe3}) ppm.

Crystal data for 1^{tBu}: $C_{25}H_{40}BFeN_2O_3P$, $M_r = 514.22$, colorless block, 0.228 × 0.225 × 0.140 mm^3, monoclinic space group $P2_1/n$, $a = 13.970(4)$ Å, $b = 13.9999(13)$ Å, $c = 15.511(5)$ Å, $\beta = 113.786(18)°$, $V = 2776.0(13)$ Å^3, $Z = 4$, $\rho_{calcd} = 1.230$ g·cm^{-3}, $\mu = 0.628$ mm^{-1}, $F(000) = 1096$, $T = 100(2)$ K, $R_1 = 0.0280$, $wR_2 = 0.0647$, 5657 independent reflections [$2\theta \leq 52.744°$] and 311 parameters.

Crystal data for 1^{Tol}: $C_{31}H_{36}BFeN_2O_3P$, $M_r = 582.25$, colorless block, 0.146 × 0.112 × 0.072 mm^3, triclinic space group $P\bar{1}$, $a = 13.856(3)$ Å, $b = 15.133(3)$ Å, $c = 16.191(3)$ Å, $\alpha = 111.856(11)°$, $\beta = 100.167(14)°$, $\gamma = 100.536(16)°$, $V = 2984.4(11)$ Å^3, $Z = 4$, $\rho_{calcd} = 1.296$ g·cm^{-3}, $\mu = 0.593$ mm^{-1}, $F(000) = 1224$, $T = 100(2)$ K, $R_1 = 0.0378$, $wR_2 = 0.0831$, 12189 independent reflections [$2\theta \leq 52.744°$] and 721 parameters.

Crystal data for 1^{Cy}: $C_{29}H_{44}BFeN_2O_3P$, $M_r = 566.29$, colorless block, 0.33 × 0.229 × 0.196 mm^3, triclinic space group $P\bar{1}$, $a = 10.830(4)$ Å, $b = 10.9882(19)$ Å, $c = 14.875(5)$ Å, $\alpha = 89.102(13)°$, $\beta = 75.134(11)°$, $\gamma = 62.20(3)°$, $V = 1502.3(8)$ Å^3, $Z = 2$, $\rho_{calcd} = 1.252$ g·cm^{-3}, $\mu = 0.586$ mm^{-1}, $F(000) = 604$, $T = 100(2)$ K, $R_1 = 0.0654$, $wR_2 = 0.0880$, 5920 independent reflections [$2\theta \leq 52.042°$] and 341 parameters.

Crystal data for 2^{iPr}: $C_{30}H_{50}BFeN_4O_3P$, $M_r = 612.37$, colorless block, 0.268 × 0.153 × 0.118 mm^3, orthorhombic space group $P2_12_12_1$, $a = 11.006(5)$ Å, $b = 16.839(6)$ Å, $c = 17.923(3)$ Å, $V = 3321.6(19)$ Å^3, $Z = 4$, $\rho_{calcd} = 1.225$ g·cm^{-3}, $\mu = 0.537$ mm^{-1}, $F(000) = 1312$, $T = 100(2)$ K, $R_1 = 0.0512$, $wR_2 = 0.0718$, 6530 independent reflections [$2\theta \leq 52.04°$] and 376 parameters.

Crystal data for 2^{Cy}: $C_{42}H_{66}BFeN_4O_3P$, $M_r = 386.31$, colorless block, 0.762 × 0.504 × 0.500 mm^3, orthorhombic space group $P2_12_12_1$, $a = 11.2062(3)$ Å, $b = 16.7934(5)$ Å, $c = 22.5143(6)$ Å, $V = 4237.0(2)$ Å^3, $Z = 8$, $\rho_{calcd} = 1.211$ g·cm^{-3}, $\mu = 0.435$ mm^{-1}, $F(000) = 1664$, $T = 296(2)$ K, $R_1 = 0.0454$, $wR_2 = 0.0934$, 8347 independent reflections [$2\theta \leq 52.044°$] and 587 parameters.

Crystal data for 6^{iPr}: $C_{52}H_{90}B_4Fe_2N_6O_6Si_4$, $M_r = 1162.59$, colorless plate, 0.20 × 0.12 × 0.10 mm^3, triclinic space group $P\bar{1}$, $a = 8.9731(6)$ Å, $b = 13.5974(9)$ Å, $c = 13.8948(9)$ Å, $\alpha = 98.829(2)°$, $\beta = 98.441(2)°$, $\gamma = 102.776(2)°$, $V = 1604.76(18)$ Å^3, $Z = 1$, $\rho_{calcd} = 1.203$ g·cm^{-3}, $\mu = 0.574$ mm^{-1}, $F(000) = 620$, $T = 100(2)$ K, $R_1 = 0.0375$, $wR_2 = 0.0889$, 6305 independent reflections [$2\theta \leq 52.044°$] and 348 parameters.

Crystal data for 6^{Cy}: $C_{32}H_{53}B_2FeN_3O_3Si_2$, $M_r = 661.42$, colorless block, 0.297 × 0.282 × 0.156 mm^3, triclinic space group $P\bar{1}$, $a = 9.7685(17)$ Å, $b = 11.7189(19)$ Å, $c = 17.273(3)$ Å, $\alpha = 73.39(2)°$, $\beta = 78.365(19)°$, $\gamma = 82.58(3)°$, $V = 1850.5(6)$ Å^3, $Z = 2$, $\rho_{calcd} = 1.187$ g·cm^{-3}, $\mu = 0.506$ mm^{-1}, $F(000) = 708$, $T = 100(2)$ K, $R_1 = 0.0745$, $wR_2 = 0.0948$, 7276 independent reflections [$2\theta \leq 52.034°$] and 462 parameters.

Crystal data for 7^{iPr}: $C_{26}H_{45}B_2FeN_3O_3Si_2$, $M_r = 581.30$, red block, $0.307 \times 0.245 \times 0.156$ mm^3, triclinic space group $P\bar{1}$, $a = 12.868(4)$ Å, $b = 17.011(3)$ Å, $c = 17.068(3)$ Å, $\alpha = 115.974(5)°$, $\beta = 91.082(16)°$, $\gamma = 101.413(11)°$, $V = 3268.6(14)$ Å^3, $Z = 4$, $\rho_{calcd} = 1.181$ g·cm^{-3}, $\mu = 0.564$ mm^{-1}, $F(000) = 1240$, $T = 100(2)$ K, $R_1 = 0.0569$, $wR_2 = 0.0942$, 13356 independent reflections [$2\theta \leq 52.744°$] and 695 parameters.

Crystal data for 7^{Cy}: $C_{35}H_{60}B_2FeN_3O_3Si_2$, $M_r = 704.51$, red block, $0.542 \times 0.246 \times 0.227$ mm^3, triclinic space group $P\bar{1}$, $a = 11.0868(9)$ Å, $b = 14.0726(9)$ Å, $c = 14.3688(9)$ Å, $\alpha = 62.807(2)°$, $\beta = 82.496(2)°$, $\gamma = 88.618(2)°$, $V = 1975.4(2)$ Å^3, $Z = 2$, $\rho_{calcd} = 1.184$ g·cm^{-3}, $\mu = 0.478$ mm^{-1}, $F(000) = 758$, $T = 100(2)$ K, $R_1 = 0.0884$, $wR_2 = 0.0975$, 7784 independent reflections [$2\theta \leq 52.044°$] and 455 parameters.

Crystal data for 8^{iPr}: $C_{26}H_{45}B_2FeN_3O_3Si_2$, $M_r = 581.30$, orange block, $0.226 \times 0.208 \times 0.096$ mm^3, monoclinic space group $P2_1/n$, $a = 9.3770(17)$ Å, $b = 20.429(3)$ Å, $c = 16.292(6)$ Å, $\beta = 90.50(3)°$, $V = 3120.8(13)$ Å^3, $Z = 4$, $\rho_{calcd} = 1.237$ g·cm^{-3}, $\mu = 0.590$ mm^{-1}, $F(000) = 1240$, $T = 109(2)$ K, $R_1 = 0.0444$, $wR_2 = 0.0984$, 6376 independent reflections [$2\theta \leq 52.744°$] and 347 parameters.

Crystal data for $9^{tBu}\cdot 11^{tBu}$: $C_{27}H_{40}BFeN_3O_3 \cdot [C_{20}H_{54}B_2N_4Si_4]_{0.5}$, $M_r = 763.61$, colorless plate, $0.231 \times 0.188 \times 0.155$ mm^3, triclinic space group $P\bar{1}$, $a = 9.379(2)$ Å, $b = 10.203(2)$ Å, $c = 24.611(4)$ Å, $\alpha = 83.324(14)°$, $\beta = 89.302(14)°$, $\gamma = 70.915(15)°$, $V = 2209.7(8)$ Å^3, $Z = 2$, $\rho_{calcd} = 1.148$ g·cm^{-3}, $\mu = 0.433$ mm^{-1}, $F(000) = 824$, $T = 100(2)$ K, $R_1 = 0.0420$, $wR^2 = 0.0854$, 8708 independent reflections [$2\theta \leq 52.044°$] and 593 parameters.

Crystal data for 3^{tBu}: $C_{56}H_{88}B_4N_4$, $M_r = 860.54$, colorless plate, $0.210 \times 0.115 \times 0.045$ mm^3, triclinic space group $P\bar{1}$, $a = 8.725(9)$ Å, $b = 8.934(8)$ Å, $c = 17.158(17)$ Å, $\alpha = 99.96(3)°$, $\beta = 94.43(3)°$, $\gamma = 94.43(3)°$, $V = 1308(2)$ Å^3, $Z = 1$, $\rho_{calcd} = 1.093$ g·cm^{-3}, $\mu = 0.061$ mm^{-1}, $F(000) = 472$, $T = 100(2)$ K, $R_1 = 0.1343$, $wR^2 = 0.3866$, 5132 independent reflections [$2\theta \leq 52.044°$] and 304 parameters.

Crystal data for 3^{SiMe3}: $C_{26}H_{44}B_2N_2Si_2$, $M_r = 462.43$, colorless block, $0.343 \times 0.142 \times 0.116$ mm^3, monoclinic space group $C2/c$, $a = 22.081(6)$ Å, $b = 9.192(3)$ Å, $c = 15.121(7)$ Å, $\beta = 109.96(2)°$, $V = 2884.6(18)$ Å^3, $Z = 4$, $\rho_{calcd} = 1.065$ g·cm^{-3}, $\mu = 0.139$ mm^{-1}, $F(000) = 1008$, $T = 100(2)$ K, $R_1 = 0.0422$, $wR^2 = 0.1036$, 2933 independent reflections [$2\theta \leq 52.726°$] and 152 parameters.

Crystal data for 11^{tBu}: $C_{20}H_{54}B_2N_4Si_4$, $M_r = 484.65$, colorless block, $0.241 \times 0.149 \times 0.094$ mm^3, Triclinic space group $P\bar{1}$, $a = 8.572(4)$ Å, $b = 9.285(6)$ Å, $c = 10.764(5)$ Å, $\alpha = 93.546(17)°$, $\beta = 104.033(12)°$, $\gamma = 112.53(2)°$, $V = 756.2(7)$ Å^3, $Z = 1$, $\rho_{calcd} = 1.064$ g·cm^{-3}, $\mu = 0.211$ mm^{-1}, $F(000) = 268$, $T = 100(2)$ K, $R_1 = 0.0841$, $wR_2 = 0.1446$, 2989 independent reflections [$2\theta \leq 52.042°$] and 145 parameters.

Crystal data for 13^{SiMe3}: $C_{22}H_{49}B_2N_3Si_4$, $M_r = 489.62$, colorless block, $0.208 \times 0.169 \times 0.146$ mm^3, monoclinic space group $P2/n$, $a = 8.7149(9)$ Å, $b = 14.234(3)$ Å, $c = 12.4968(15)$ Å, $\beta = 96.522(13)°$, $V = 1540.2(4)$ Å^3, $Z = 2$, $\rho_{calcd} = 1.056$ g·cm^{-3}, $\mu = 0.207$ mm^{-1}, $F(000) = 536$, $T = 100(2)$ K, $R_1 = 0.0327$, $wR_2 = 0.0841$, 3144 independent reflections [$2\theta \leq 52.734°$] and 151 parameters.

Deposition Numbers 2096717 ($\mathbf{1}^{Cy}$), 2096718 ($\mathbf{6}^{Cy}$), 2096719 ($\mathbf{2}^{Cy}$), 2096720 ($\mathbf{6}^{iPr}$), 2096721 ($\mathbf{8}^{iPr}$), 2096722 ($\mathbf{1}^{Tol}$), 2096723 ($\mathbf{9}^{tBu}\cdot\mathbf{11}^{tBu}$), 2096724 ($\mathbf{13}^{SiMe3}$), 2096725 ($\mathbf{7}^{iPr}$), 2096726 ($\mathbf{7}^{Cy}$), 2096727 ($\mathbf{11}^{tBu}$), 2096728 ($\mathbf{1}^{tBu}$), 2096729 ($\mathbf{3}^{tBu}$), 2096730 ($\mathbf{2}^{iPr}$), and 2096731 ($\mathbf{3}^{SiMe3}$) contain the supplementary crystallographic data for this paper. These data are provided free of charge by the joint Cambridge Crystallographic Data Centre and Fachinformationszentrum Karlsruhe Access Structures service www.ccdc.cam.ac.uk/structures.

Acknowledgements

Funding from the Deutsche Forschungsgemeinschaft (DFG) is gratefully acknowledged. F.S. thanks the Studienstiftung des Deutschen Volkes for a Ph.D. scholarship. Open Access funding enabled and organized by Projekt DEAL.

Conflict of Interest

The authors declare no conflict of interest.

Keywords: Borylene complexes · Cycloaddition · Metathesis · Reaction mechanisms · Structure elucidation

[1] a) A. H. Cowley, V. Lomelí, A. Voigt, *J. Am. Chem. Soc.* **1998**, *120*, 6401–6402; b) H. Braunschweig, C. Kollann, U. Englert, *Angew. Chem. Int. Ed.* **1998**, *37*, 3179–3180; *Angew. Chem.* **1998**, *110*, 3355–3357.
[2] a) J. T. Goettel, H. Braunschweig, *Coord. Chem. Rev.* **2019**, *380*, 184–200; b) H. Braunschweig, R. D. Dewhurst, V. H. Gessner, *Chem. Soc. Rev.* **2013**, *42*, 3197–3208; c) D. Vidovic, G. A. Pierce, S. Aldridge, *Chem. Commun.* **2009**, 1157–1171; d) C. E. Anderson, H. Braunschweig, R. D. Dewhurst, *Organometallics* **2008**, *27*, 6381–6389.
[3] a) D. L. Kays, J. K. Day, L.-l. Ooi, S. Aldridge, *Angew. Chem. Int. Ed.* **2005**, *44*, 7457–7460; *Angew. Chem.* **2005**, *117*, 7623–7626; b) D. L. Kays, A. Rossin, J. K. Day, L.-l. Ooi, S. Aldridge, *Dalton Trans.* **2006**, 399–410.
[4] J. Bauer, H. Braunschweig, A. Damme, J. O. C. Jimenez-Halla, T. Kramer, K. Radacki, R. Shang, E. Siedler, Q. Ye, *J. Am. Chem. Soc.* **2013**, *135*, 8726–8734.
[5] H. Braunschweig, M. Burzler, K. Radacki, F. Seeler, *Angew. Chem. Int. Ed.* **2007**, *46*, 8071–8073; *Angew. Chem.* **2007**, *119*, 8217–8219.
[6] H. Braunschweig, K. Radacki, Q. Ye, *Chem. Commun.* **2012**, *48*, 2701–2703.
[7] a) J. Niemeyer, M. J. Kelly, I. M. Riddlestone, D. Vidovic, S. Aldridge, *Dalton Trans.* **2015**, *44*, 11294–11305; b) G. A. Pierce, D. Vidovic, D. L. Kays, N. D. Coombs, A. L. Thompson, E. D. Jemmis, S. De, S. Aldridge, *Organometallics* **2009**, *28*, 2947–2960.
[8] a) G. A. Pierce, N. D. Coombs, D. J. Willock, J. K. Day, A. Stasch, S. Aldridge, *Dalton Trans.* **2007**, 4405–4412; b) G. A. Pierce, S. Aldridge, C. Jones, T. Gans-Eichler, A. Stasch, N. D. Coombs, D. J. Willock, *Angew. Chem. Int. Ed.* **2007**, *46*, 2043–2046; *Angew. Chem.* **2007**, *119*, 2089–2092; c) S. De, G. A. Pierce, D. Vidovic, D. L. Kays, N. D. Coombs, E. D. Jemmis, S. Aldridge, *Organometallics* **2009**, *28*, 2961–2975.
[9] B. Borthakur, H. Braunschweig, A. Deißenberger, T. Dellermann, R. D. Dewhurst, I. Krummenacher, M. Nutz, A. K. Phukan, M. Schäfer, *Angew. Chem. Int. Ed.* **2017**, *56*, 7975–7979; *Angew. Chem.* **2017**, *129*, 8084–8089.
[10] a) H. Braunschweig, J. O. C. Halla, K. Radacki, R. Shang, *Angew. Chem. Int. Ed.* **2016**, *55*, 12673–12677; *Angew. Chem.* **2016**, *128*, 12864–12868; b) H. Braunschweig, T. Herbst, K. Radacki, C. W. Tate, A. Vargas, *Chem. Commun.* **2013**, *49*, 1702–1704.
[11] H. Braunschweig, Q. Ye, A. Vargas, R. D. Dewhurst, K. Radacki, A. Damme, *Nat. Chem.* **2013**, *5*, 88–89.
[12] H. Braunschweig, A. Damme, K. Radacki, A. Vargas, Q. Ye, *Angew. Chem. Int. Ed.* **2013**, *52*, 10657–10660; *Angew. Chem.* **2013**, *125*, 10851–10854.
[13] H. Braunschweig, Q. Ye, K. Radacki, A. Damme, *Angew. Chem. Int. Ed.* **2012**, *51*, 7839–7842; *Angew. Chem.* **2012**, *124*, 7959–7962.
[14] H. Braunschweig, Q. Ye, M. A. Celik, K. Radacki, R. D. Dewhurst, *Angew. Chem. Int. Ed.* **2015**, *54*, 5065–5068; *Angew. Chem.* **2015**, *127*, 5154–5157.
[15] H. Braunschweig, R. D. Dewhurst, K. Radacki, B. Wennemann, Q. Ye, *Chem. Commun.* **2015**, *51*, 15465–15468.
[16] T. Franz, E. Hanecker, H. Nöth, W. Stöcker, W. Storch, G. Winter, *Chem. Ber.* **1986**, *119*, 900–916.
[17] H. Braunschweig, R. D. Dewhurst, C. Schneider, *Organometallics* **2016**, *35*, 1002–1007.
[18] H. Braunschweig, R. D. Dewhurst, F. Hupp, C. Kaufmann, A. K. Phukan, C. Schneider, Q. Ye, *Chem. Sci.* **2014**, *5*, 4099–4104.

[19] P. Paetzold, A. Richter, T. Thijssen, S. Würtenberg, *Chem. Ber.* **1979**, *112*, 3811–3827.
[20] a) H. V. Ly, T. D. Forster, D. Maley, M. Parvez, R. Roesler, *Chem. Commun.* **2005**, 4468–4470; b) H. V. Ly, T. D. Forster, A. M. Corrente, D. J. Eisler, J. Konu, M. Parvez, R. Roesler, *Organometallics* **2007**, 26, 1750–1756; c) H. V. Ly, J. Moilanen, H. M. Tuononen, M. Parveza, R. Roesler, *Chem. Commun.* **2011**, *47*, 8391–8393.
[21] a) J. Schulze, G. Schmid, *Angew. Chem.* **1980**, *92*, 61–62; *Angew. Chem. Int. Ed.* **1980**, *19*, 54–55; b) J. Schulze, R. Boese, G. Schmid, *Chem. Ber.* **1980**, *113*, 2348–2357.
[22] K.-H. v Bonn, T. v Bennigsen-Mackiewicz, J. Kiesgen, C. v Plotho, P. Paetzold, *Z. Naturforsch.* **1988**, *43b*, 61–68.
[23] P. Paetzold, E. Schröder, G. Schmid, R. Boese, *Chem. Ber.* **1985**, *118*, 3205–3216.
[24] K. Halbauer, D. Dönnecke, H. Görls, W. Imhof, *Z. Anorg. Allg. Chem.* **2006**, *632*, 1477–1482.
[25] H. Hess, *Acta Crystallogr.* **1969**, *B25*, 2342–2349.
[26] a) T. C. Forschner, A. R. Cutler, *Organometallics* **1985**, *4*, 1247–125; b) S. L. Brown, S. G. Davies, *J. Chem. Soc. Chem. Commun.* **1986**, *1*, 84–85; c) X.-F. Wu, X. Fang, L. Wu, R. Jackstell, H. Neumann, M. Beller, *Acc. Chem. Res.* **2014**, *47*, 1041–1053.
[27] a) J. Zhu, Z. Lin, T. B. Marder, *Inorg. Chem.* **2005**, *44*, 9384–9390; b) H. Braunschweig, P. Brenner, A. Müller, K. Radacki, D. Rais, K. Uttinger, *Chem. Eur. J.* **2007**, *13*, 7171–7176.
[28] S. Berski, Z. Latajkaa, A. J. Gordona, *New J. Chem.* **2011**, *35*, 89–96.
[29] a) J. L. Martinez, S. A. Lutz, H. Yang, J. Xie, J. Telser, B. M. Hoffman, V. Carta, M. Pink, Y. Losovyj, J. M. Smith, *Science* **2020**, *370*, 356–359; b) Z. Ouyang, L. Deng, *Organometallics* **2013**, *32*, 7268–7271.
[30] a) T. Renk, W. Ruf, W. Siebert, *J. Organomet. Chem.* **1976**, *120*, 1–25; b) A. Appel, F. Jäkle, T. Priermeier, R. Schmid, M. Wagner, *Organometallics* **1996**, *15*, 1188–1194; c) L. Kaufmann, H. Vitze, M. Bolte, H.-W. Lerner, M. Wagner, *Organometallics* **2008**, *27*, 6215–6221; d) B. Wrackmeyer, U. Dörfler, W. Milius, M. Herberhold, *Polyhedron* **1995**, *14*, 1425–1431; e) A. Appel, H. Nöth, M. Schmidt, *Chem. Ber.* **1995**, *128*, 621–626; f) M. Scheibitz, M. Bolte, J. W. Bats, H.-W. Lerner, J. Nowik, R. H. Herber, A. Krapp, M. Lein, M. C. Holthausen, M. Wagner, *Chem. Eur. J.* **2005**, *11*, 584–603; g) H. Braunschweig, I. Fernández, G. Frenking, T. Kupfer, *Angew. Chem. Int. Ed.* **2008**, *47*, 1951–1954; *Angew. Chem.* **2008**, *120*, 1977–1980; h) H. Braunschweig, C.-W. Chiu, D. Gamon, M. Kaupp, I. Krummenacher, T. Kupfer, R. Müller, K. Radacki, *Chem. Eur. J.* **2012**, *18*, 11732–11746.
[31] I. Bernal, H. Vogt, *J. Organomet. Chem.* **1995**, *502*, 103–108.
[32] G. Sheldrick, *Acta Crystallogr.* **2015**, *A71*, 3–8.
[33] G. Sheldrick, *Acta Crystallogr.* **2008**, *A64*, 112–122.
[34] K. Halbauer, D. Dönnecke, H. Görls, W. Imhof, *Z. Anorg. Allg. Chem.* **2006**, *632*, 1477–1482.

Manuscript received: July 21, 2021
Revised manuscript received: August 31, 2021
Accepted manuscript online: September 3, 2021